



**SUM-FREQUENCY GENERATION  
AND MULTIPHOTON IONIZATION  
IN XENON UNDER EXCITATION  
BY CONICAL LASER BEAMS**

**SERGEY SHCHEMELYOV**



TARTU UNIVERSITY  
**PRESS**

The study was carried out at the Institute of Physics of the University of Tartu.

The Dissertation was admitted on June 28, 2006, in partial fulfillment of the requirements for the degree of Doctor of Philosophy in physics (optics and spectroscopy), and allowed for defence by the Council of Department of Physics, University of Tartu.

Supervisor: Victor Peet, PhD, Institute of Physics, University of Tartu

Opponents: Anatoly Isaev, Dr Sc, P. N. Lebedev Physical Institute of Russian Academy of Sciences, Laboratory of Physical Optics, leading scientist

Ilmo Sildos, PhD, Head of Laboratory of Laser Spectroscopy,  
Institute of Physics, University of Tartu

Defence: September 13, 2006, at University of Tartu, Tartu, Estonia

ISSN 1406–0647

ISBN 9949–11–422–5 (trükis)

ISBN 9949–11–423–3 (PDF)

Autoriõigus Sergey Shchemelyov, 2006

Tartu Ülikooli Kirjastus

[www.tyk.ee](http://www.tyk.ee)

Tellimuse nr 400

# CONTENTS

LIST OF PUBLICATIONS.....	6
1. INTRODUCTION.....	8
2. TH GENERATION IN CONICAL BEAMS: GENERAL BACKGROUND.....	13
3. EXPERIMENTAL SETUP .....	16
4. TH GENERATION AND MULTIPHOTON IONIZATION IN CONICAL LASER BEAMS.....	19
4.1. Results and discussion.....	20
4.2. Numerical simulation of the TH profiles.....	28
5. SPATIALLY INCOHERENT LASER BEAMS .....	34
5.1. Experimental arrangement.....	34
5.2. Four-wave mixing in spatially incoherent laser beams .....	37
5.3. Analysis of spectral profiles .....	41
6. SPATIALLY INCOHERENT CONICAL LASER BEAMS.....	46
6.1. Characterization of incoherent conical beams.....	46
6.2. Experimental results with incoherent conical beams.....	49
6.3. Analysis of experimental profiles.....	52
7. CONCLUSION .....	58
SUMMARY.....	62
SUMMARY IN ESTONIAN .....	63
REFERENCES .....	64

## LIST OF PUBLICATIONS

This thesis is based on the following papers:

- I. V. Peet, W. R. Garrett and S. Shchemel'gov, Near-resonance three-photon excitation profiles in xenon with segmented conical beams, *Phys. Rev.*, **A63**, 023804 (5 pp), 2001.
- II. V. Peet and S. Shchemel'gov, Spectral and spatial characteristics of third-harmonic generation in conical light beams, *Phys. Rev.*, **A67**, 013801 (7 pp), 2003.
- III. V. Peet and S. Shchemel'gov, Three-photon resonant atomic excitation in spatially incoherent laser beams, *Phys. Rev.*, **A68**, 043411 (8 pp), 2003.
- IV. V. Peet and S. Shchemel'gov, Sum-frequency generation and multiphoton ionization in spatially incoherent conical laser beams, *Opt. Commun.*, **246**, pp 451–463, 2005.

The following papers are related to the subject of the thesis:

V. Peet, W. R. Garrett, and S. Shchemel'gov, Generation of resonance-enhanced third harmonic in Bessel and segmented Bessel beams, Digest Int. Quantum Electronic Conf. IQEC/Europe'2000, p. 209, Nice, France, 2000.

V. Peet, W. R. Garrett, and S. Shchemel'gov, Resonance-enhanced multiphoton excitation and ionization of rare gases in conical laser beams, Abstr. Int. Spectroscopy Conf. CSI XXXII, pp 4–10, Pretoria, South Africa, 2001.

V. Peet, R. Tsubin, and S. Shchemel'gov, Generation of low-order harmonics in rare gases with non-Gaussian laser beams, In: ICO XIX: Optics for the Quality of Life, A. Consortini and G. S. Righini, Editors, Proc. SPIE 4829, pp 391–392, Firenze, Italy, 2002.

S. Shchemel'gov and V. Peet, Generation of resonance-enhanced third harmonic in conical laser beams, Second Scientific School for Young Scientists "Optics-2002", pp 76–77, Saint-Petersburg, Russia, 2002.

V. Peet and S. Shchemel'gov, Resonance-enhanced multiphoton processes in incoherent light field, Abstr. 16th Int. Conf. "Laser Spectroscopy" ICOLS 03, p.201, Palm Cove, Queensland, Australia, 2003.

S. Shchemel'gov and V. Peet, Spatially incoherent laser beams in multiphoton resonance-enhanced ionization of xenon, III International Conference for Students, Young Scientists and Engineers "Optics 2003", Postdeadline Section, Saint-Petersburg, Russia, p. 7, 2003.

V. Peet and S. Shchemel'ov, Coherent wave-mixing processes and multiphoton ionization in spatially incoherent conical laser beams, Abstr. 28<sup>th</sup> Europ. Conf. on Laser Interaction with Matter, Rome, Italy, p. 141, 2004.

S. Shchemel'ov and V. Peet, Multiphoton processes in spatially incoherent conical laser beams, Abstr. IV Int. Young Scientist Conf. "Optics-2005", Saint-Petersburg, Russia, p. 20, 2005.

# 1. INTRODUCTION

The problem of interaction of intense laser light with matter has been of great and permanent interest due to fundamental problems of light-matter interaction and a variety of applications of lasers in optics, spectroscopy, technologies, etc. The output emission of lasers is usually transported in a form of so-called Gaussian beams, where the amplitude profile is close to a Gaussian one. Thus, the most of experimental and theoretical studies on laser beam interaction with matter until the late 1980's were carried out just for Gaussian beams.

Last years several novel types of light beams have been introduced both theoretically and experimentally. These non-traditional beams have, in general, the field amplitude and phase profiles essentially different from the ordinary Gaussian beams. Among novel types of laser beams, the so-called diffraction-free beams are of great interest. In 1987 a new type of such beams as solutions to the homogeneous Helmholtz equation was introduced by Durnin [1] and, soon afterwards, realized experimentally [2]. These beams have become known as Bessel beams owing to their transverse structure given by Bessel function  $J_0$  of the first kind and order zero. Actually, light field profiles described by  $J_0$  Bessel functions are well known in classical optics, but less attention was paid until recently to the field depth. Durnin and co-workers just pointed to a very unusual feature of Bessel light fields. Namely, the Bessel beams give high concentration of light energy into a small spot but the spot size remains nearly constant over a distance of propagation, which can be made much larger than the Rayleigh length of a focused Gaussian beam. The intensity profile of such propagation-invariant beams does not depend on the coordinate in propagation direction, but only on the transverse coordinate. Thus, the Bessel beams introduced into optics the concept of propagation-invariant or diffraction-free light fields. This feature makes the Bessel beams very attractive for a variety of applications where enlarged propagation depth is required.

Initially, the research into applications of Bessel beams was focused essentially on the nondiffracting aspect, concentrating on various experimental realizations and investigating about the length of diffraction-free propagation [3]. In original experiment by Durnin and co-workers [2] the Bessel beam was created by placing a thin circular slit in the focal plane of a lens. Later several other methods were introduced, where the desired diffraction-free Bessel beams were obtained with the aid of spherical lenses [4], confocal resonator with an annular active medium [5], holographic methods [6 – 10], Fabry-Perot interferometers [11, 12], and periodic gratings with circular symmetry [13 – 15]. The most effective method for producing Bessel beams, however, is based

on the use of conical optical elements or axicons. Axicon lens transforms the incident laser beam into a cone of plane waves behind the axicon, where the interference pattern is the desired Bessel beam. Since 1970 this simple and effective method is used in experiments with extended excitation regions [16 – 19].

Physically realizable Bessel and Gaussian beams are actually special cases of a general Bessel-Gauss beam, which appears as a solution of paraxial wave equation [20 – 28]. In experiments, the incident laser beam has in most cases a Gaussian transverse profile and the produced Bessel beam is naturally cut-off in the transverse direction by the exponentially decaying Gaussian profile. Under axicon focusing with relatively large inclination angle, dominating is the Bessel profile since the Gaussian envelope is usually much broader. An interesting and useful realization of a Bessel-Gauss profile can be obtained with the use of annular laser beams focused by an ordinary spherical lens [29 – 33]. In this case, the field profile in the focal region resembles very much the central part of a Bessel beam, but with suppressed outer oscillations of the Bessel function. Such method does not require special conical optics, but allows one to get conical excitation geometry similar to the Bessel beams.

Bessel beam can be considered as a superposition of infinitely many plane waves whose wave vectors form a conical surface. For a  $J_0$  Bessel beam all these plane waves have equal amplitudes and phases. Besides zero-order  $J_0(r)$  Bessel beams, there is a family of higher-order  $J_m(r)$  beams ( $m = 1, 2, 3$ , etc.), where the phase of partial plane waves changes in azimuthal direction [9, 34 – 37]. All these Bessel beams are “nondiffractive” in the same sense, but in contrast to  $J_0(r)$  beams all higher-order Bessel beams have intensity minimum on their axes. Other examples of new types of conical laser beams are segmented beams [38], Mathieu beams [39 – 42], and truncated Bessel beams [43, 44]. These conical beams share the propagation properties of Bessel beams, but they have amplitude profiles different from the Bessel pattern. Segmented conical beams [38] remain propagation-invariant in the same sense as the initial Bessel beam, i.e. the transverse profile of a segmented beam remains nearly unchanged along the propagation distance. Recently it was shown [39 – 42] that some of segmented conical beams represent a new type of propagation-invariant light fields, where the field distribution is described by radial and angular Mathieu functions. These Mathieu beams appear as solutions to the Helmholtz equation in elliptic coordinates [39 – 41]. In contrast to the Bessel beams, the transverse profiles of Mathieu beams consist of several lobes, where the light is concentrated [39 – 42].

Interesting novel beams are modified Bessel beams of I-type [45]. Existence of such concave beams as a solution to the three-dimensional wave equation has



been shown in [45], but no experimental realization of such beams has been reported so far. Remarkable feature of modified Bessel beams is that they possess the phase velocity smaller than the speed of light  $c$  in contrast to the ordinary J-beams, where the phase velocity always is larger than  $c$ . I-type Bessel beams have a negative phase lag (reverse Guoy effect) in contrast to the J-type Bessel and focused Gaussian beams [45]. These features of I-type Bessel beams may lead to several interesting and unusual effects in nonlinear optics, where the phase matching of interacting waves is of great importance.

In all above examples the conical light field is characterized by a complete spatial coherence when all partial waves maintain their mutual correlation under propagation. Another class of propagation-invariant light fields includes partially coherent conical beams. Special case of such beams is represented by the so-called Bessel-correlated beams [46], where correlation between individual plane waves vanishes in azimuthal direction. Conical superposition of such mutually uncorrelated plane waves produces a propagation-invariant intensity profile, as well. In a stationary case of partial azimuthal incoherence the field profile of Bessel-correlated beams is decomposed into multiple irregular speckles, which preserve their location and shape under propagation. In other words, such partially coherent conical beam is comprised of multiple parallel light filaments distributed irregularly within the beam profile and extended along the beam axis. In general, both azimuthal and radial incoherence can be introduced into conical superposition of multiple plane waves. It allows one to synthesize a variety of specific field configurations like, for example, light strings and light capillary beams [47, 48].

Interesting and unusual properties of novel laser beams are especially attractive for nonlinear optics, where such beams often demonstrate significant difference as compared with ordinary Gaussian beams. The field of nonlinear optics originates from 1961, when the second-harmonic generation of optical emission was observed by Franken and coworkers [49] shortly after demonstration of the first ruby laser. Interest in this field has grown continuously since beginning, and the field of nonlinear optics now ranges from fundamental studies of light-matter interaction to a variety of applications such as laser frequency conversion, material processing, telecommunications, and others. Nonlinear optical phenomena are “nonlinear” in the sense that they occur when the response of a material system to an applied optical field depends in a nonlinear manner upon the strength of the optical field. For example, the lowest-order nonlinear process such as second-harmonic generation occurs as a result of atomic response that depends quadratically on the strength of applied optical field. In gases and other media with inversion center any even harmonics

are not generated. In such media, an intense laser field of frequency  $\omega$  induces polarization where alongside with linear polarization at frequency  $\omega$  additional nonlinear components at frequencies  $3\omega$ ,  $5\omega$ , etc. appear. Induced nonlinear polarization becomes a source of radiation at the corresponding frequencies. Nowadays the harmonic generation in gases and crystals is a well-established and continuously expanding field of nonlinear optics. One of such frequency conversion methods employs generation of third harmonic (TH)  $3\omega$  in gaseous media and it has long been established as a method for generation of coherent radiation in the UV and VUV regions where the number of available laser sources is very limited. Frequency tripling in the TH generation process represents a special case of nonlinear four-wave mixing (FWM), where nonlinear susceptibility  $\chi^{(3)}$  of the medium couples three fundamental fields of frequency  $\omega$  and the generated TH field at  $3\omega$ .

Very interesting properties of Bessel beams have made the initial researches for a long time be focused essentially on the nondiffracting aspect of these beams, but it took much longer to appreciate the possibility of using the Bessel and other novel beams in optimizing nonlinear optical processes. The first demonstration of Bessel beams in generation of second harmonics in a nonlinear crystal was reported in [50]. It has been shown there that with Bessel beams the phase-matching condition for optimum harmonic generation is not limited to one direction (that is, the propagation direction) but can be tuned continuously by varying the inclination angle of the Bessel beam. Very much at the same time similar results were obtained using excitation by Bessel-like conical beams in generation of TH in metal vapors [29]. It has been demonstrated, that with the use of the conical excitation geometry of a Bessel beam, the harmonic output can be increased by several times together with certain immunity of harmonic output to variations of excitation conditions. Further studies of Bessel beams in nonlinear optics have revealed incrementally other very interesting and potentially useful properties of such novel beams in initiation of different nonlinear processes [51 – 75].

In most researches on nonlinear optics with Bessel and other conical beams, the simplest coherent beams like  $J_0$  Bessel beams were usually used, but much less is known about nonlinear optical processes driven by incoherent conical beams. In the process of a nonlinear conversion of the fundamental laser light the incoherent beams are usually considered as less attractive since the presence of wave-front irregularities reduces the length of coherent nonlinear interaction and leads to significant destructive interference of secondary emission from multiple uncorrelated regions. However, it has been demonstrated recently that conical excitation geometry allows one to preserve a relatively high conversion

efficiency in the process of optical parametric oscillations even for a pumping beam with significantly degraded spatial coherence [76]. Such a tolerance may be very interesting and useful feature of conical beams in the excitation of nonlinear optical processes.

For intense laser beams the process of TH generation is accompanied by multiphoton excitation and ionization of the target gas atoms. These processes change the properties of gaseous medium and the onset of intense ionization is one of the limiting factors for tripling efficiency. On the other hand, gas-phase multiphoton excitation and resonance-enhanced multiphoton ionization (REMPI) are effective and widespread techniques of modern laser spectroscopy. A large number of experimental and theoretical works on REMPI have shown the importance of harmonics of the fundamental light in the response of atomic system under excitation (see, for example, [77 – 90] and references therein). The harmonic field, once generated, becomes an additional source of coherent excitation of the target gas atoms. The excitation pathways, where the harmonic and fundamental photons are involved, may interfere constructively or destructively and it leads to strong enhancement or suppression of multiphoton excitation and ionization processes. Until recently these very complicated processes were studied with Gaussian beams but much less is known about peculiarities of these processes under excitation by novel types of laser beams.

In the present work, the conical laser beams were used to study the generation of resonance-enhanced sum-frequency field in gaseous medium together with accompanying processes of multiphoton excitation and ionization of the target gas atoms. This study was not aimed toward any optimization of sum-frequency generation efficiency, but special attention was paid to understanding the peculiarities of conical laser beams in excitation of nonlinear optical processes. These investigations included the following tasks:

- generation of resonance-enhanced TH in the lowest-order Bessel and segmented conical beams; the role of harmonic photons in multiphoton excitation and ionization of the target gas.
- generation of resonance-enhanced sum-frequency field under mixed two-color excitation by coherent and incoherent conical laser beams; comparison of analogous result with the case of ordinary Gaussian beams.
- analysis and numerical simulation of TH and sum-frequency excitation profiles in different conical beams.

## 2. TH GENERATION IN CONICAL BEAMS: GENERAL BACKGROUND

The field distribution in a zero-order Bessel and other conical beams results from a superposition of multiple plane waves all inclined by a constant angle  $\alpha$  toward the propagation axis. For a single plane wave the field of generated harmonic consists of two components [91 – 95]. The first is a free wave propagating with the phase velocity at the harmonic frequency and another component is the driven wave, which propagates with the phase velocity of the fundamental wave. Microscopic partial waves generated by individual atoms or molecules in various points of the nonlinear medium give a macroscopic wave of significant intensity only in the case, when phase velocities of both the induced and the free waves are equal. This collinear phase-matching condition is written as:

$$k(3\omega) = 3k(\omega), \quad (1)$$

where  $k(\omega)$  and  $k(3\omega)$  are the wave vectors of radiation at frequencies  $\omega$  and  $3\omega$ , respectively. The phase matching condition (1) follows from the momentum conservation law for photons participating in the TH generation process.

Mismatch of the wave vectors in the TH generation is given by expression

$$\Delta k = k_3 - 3k_1 = (6\pi / \lambda)(n_3 - n_1), \quad (2)$$

where  $n_i$  is the refraction index at frequency  $\omega_i$ . Due to dispersion of refraction indices  $n_i$ , the pump and the TH waves have, in general, different phase velocities. It results in an interference, which either strengthens or weakens the macroscopic TH in different areas of the nonlinear medium. The maximum TH output is achieved when  $\Delta k = 0$ . It is the case of a complete phase matching realized when refraction indices at both frequencies are equal:  $n_3 = n_1$ .

In the case of a finite phase mismatch the TH intensity is reduced with respect to its value at  $\Delta k = 0$  and oscillates along the propagation axis. Such behavior of intensity is caused by gradual increase of phase mismatch between the TH and the driven nonlinear polarization

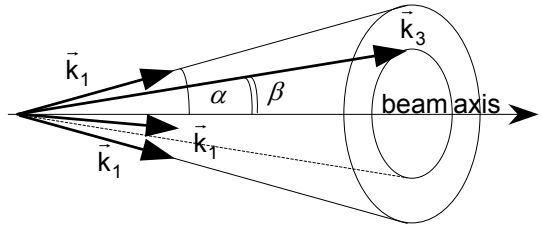


**Figure 1.** Wave-vector diagram for the TH generation in conical beams.

at propagation of waves through the medium. Alternatively, this effect can be considered as a result of constructive and destructive interference between the free and the driven waves.

The Bessel and the other conical beams realize noncollinear interaction of multiple plain waves. This case is more complicated for analysis, since the number of interacting waves becomes infinite. Due to axial symmetry, the TH radiation in a Bessel beam has the form of an outgoing cone with an inclination angle  $\beta$  (Fig. 1). Depending on excitation conditions the angle  $\beta$  can be changed from 0 to  $\alpha$ . In the former case the TH radiation is directed along the beam axis. In the latter case, the TH cone coincides the fundamental cone of radiation at frequency  $\omega$ . These two limiting cases determine the range of experimental conditions when the phase-matched TH can be generated in conical beams.

Due to noncollinear interaction of multiple waves in conical beams, the so-called mechanism of self-phase-matching (SPM) can be realized in the TH generation process [29 – 31]. Experiments with conical excitation geometry of a focused ring-shaped beam have shown the ability of supporting the phase-matched TH in a broad range of refraction index variations. Such tolerance arises because of possibility to combine different azimuthal components from the fundamental light cone to produce phase-matched TH for given excitation conditions. A theory of this SPM phenomenon was developed soon afterwards to analyze the results of [30, 31]. In this theory, the nonlinear response was derived from direct treatment of scalar wave equation with the conical source field represented as a Bessel beam. Similar approach was used in further studies on generation of low-order harmonics with Bessel beams [68, 96].

In general, noncollinear TH generation needs two phase-matching condition to be satisfied simultaneously. First, there is a condition for axial components of wave vectors (longitudinal condition). Second condition appears for the wave vector components on the plane perpendicular to the beam axis (transverse condition). For a conical beam the longitudinal phase matching condition is written similar to Eq. (1) as

$$3k(\omega)\cos\alpha = k(3\omega)\cos\beta, \quad (3)$$

The transverse phase matching condition is more complex. For a full-aperture Bessel beam this condition is given by spatial integral of the overlap of the TH Bessel beam with the cube of the fundamental Bessel beam [30, 31]. For practical applications, a more simple condition for the maximum of the TH output is usually used. This condition reads as [29 – 31]:

$$\tan \beta = \frac{1}{3} \tan \alpha . \quad (4)$$

For the nonlinear process of wave mixing the Bessel beam realizes an infinite number of possible spatial combinations of interacting waves taken with different azimuthal angles from the fundamental light cone. Each of these combinations produces its own partial contribution to the nonlinear polarization of the medium. The resulting nonlinear response of the medium is formed as a superposition of all such individual contributions. This general picture remains valid also for segmented conical beam where the range of available azimuthal angles differs from full-aperture Bessel beams. More detailed consideration of the TH generation in Bessel and segmented conical beams will be given below in section 4.

### 3. EXPERIMENTAL SETUP

Generation of sum-frequency field in conical light beams was studied with the aid of REMPI of the target gas. In this method, the gaseous medium absorbs generated photons and laser light ionizes the formed excited atoms. It is well known [81, 97, 98] that the absorption of resonance-enhanced harmonic and subsequent ionization of excited gas atoms produces ionization profiles, which closely follow the intensity of generated harmonic field. Ionization of the target gas atoms allows one to detect also the harmonic generation process in conditions of very strong absorption when no harmonic emission exits the gas cell. This advantage of REMPI method is especially important for detection of internally-generated near-resonance harmonics [77 – 79, 83, 85 – 87, 99 – 101], when propagation length for sum-frequency photons can be as short as a fraction of wavelength and these photons cannot be detected directly.

Experimental setup is shown schematically in Fig. 2. The radiation of XeCl excimer laser ELI-71 (generation wavelength 308 nm, maximum pulse energy up to 100 mJ) was used for pumping the master oscillator and the amplifier of the dye laser VL – 10.

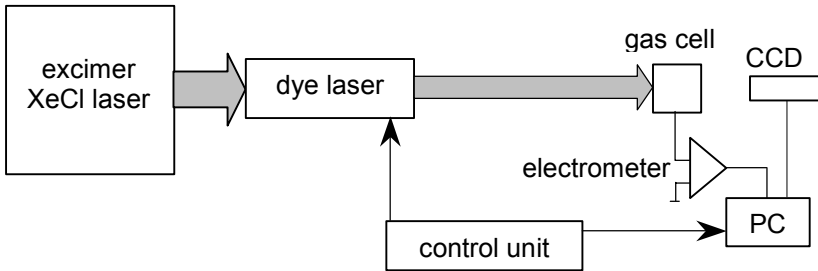


**Figure 2.** Experimental setup.

The dye laser pulses had a pulse duration of 7 – 10 ns, and spectral width of about 10 pm full width at half maximum (FWHM). Dye laser was operated with the Coumarin-120 dye in 423 – 468 nm spectral range, Rhodamine-N dye in 555 – 565 nm spectral range, or QUI dye in 388 – 389 nm spectral range.

Ionization yield under multiphoton excitation and subsequent ionization of gas atoms was measured in a static gas cell. The cell was made of stainless steel and contained xenon at a pressure of up to 3 bar. The contents of impurities in the used xenon did not exceed 0.005%. Photoelectrons resulting from multiphoton ionization process were monitored with a wire collector biased by from

+20 to +200 V. Ionization signals were amplified, digitized, and stored in a computer.

In conical excitation geometry, the laser beams were focused to the target gas by a quartz conical lens (axicon) mounted as an input window of the cell. Two different axicons with apex angles of  $120^\circ$  and  $140^\circ$  were used. Depending on laser wavelength, these axicons produced conical beams with inclination angles  $\alpha$  ranging within  $17.2-17.9^\circ$  and  $10.1-10.5^\circ$ , respectively. In most cases, small variations of inclination angles could be neglected and further the corresponding conical beams will be termed as beams with fixed inclination angles  $\alpha = 17^\circ$  and  $\alpha = 10^\circ$ . In reference experiments with Gaussian beams, a plane-parallel quartz window was mounted instead of the axicon and the laser beam was focused into the cell by either spherical lens or on-axis spherical mirror.

Spatial distribution of light intensity in the excitation region of different beams was measured with the aid of a computer-controlled 8-bit CCD camera DIC-HR (World Precision Instruments). The focal spots of used laser beams were projected by a microscope and magnified 2D images were recorded by the camera. The spectral range of CCD camera is  $400-1100$  nm, resolution  $753 \times 488$  pixels, pixel size  $8 \times 8 \mu\text{m}^2$ .

Two excitation schemes were used in experiments. The resonance-enhanced TH was generated under one-color excitation, when the beam of dye laser was focused to the gas cell. Another scheme was used in experiments on generation of sum-frequency field under mixed two-color excitation by coherent and incoherent laser beams. In this case, the dye laser was used as a source of coherent radiation  $\omega_1$  and the excimer laser served as a source of incoherent UV radiation  $\omega_2$  synchronized with the pulses of dye laser. For this purpose, a

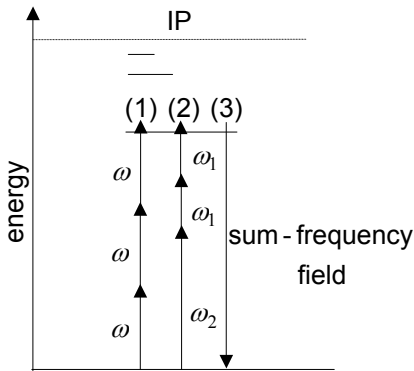


**Figure 3.** Schematic energy-level diagram of xenon and main excitation channels.

small portion of XeCl laser output was directed toward the ionization cell together with the dye laser beam. This particular excitation scheme will be considered in more details below (section 5).

Figure 3 shows a simplified energy diagram of xenon together with main excitation and ionization channels. Resonance-enhanced TH (or sum-frequency field in two-color experiments) was generated in the negatively-dispersive side of either three-photon  $6s$



resonance ( $\varepsilon = 8.44 \text{ eV}$ ) or  $6s'$  resonance ( $\varepsilon = 9.57 \text{ eV}$ ) of xenon. Generated field had the wavelength near 147 nm and near 129 nm, respectively. In one-color excitation mode (channel 1 in Fig. 3) the generated sum-frequency field (3 in Fig. 3) was the TH  $3\omega$  of the fundamental laser light. The second scheme employed two-color  $2\omega_1 + \omega_2$  excitation of the same transition (channel 2 in Fig. 3). The ionization profiles measured in such combined coherent–incoherent two-color excitation mode were compared with the profiles measured in the same conditions under coherent one-color excitation. Additionally, the results with conical beams were compared with analogous results obtained in ordinary excitation geometry of focused laser beams [102].

## 4. TH GENERATION AND MULTIPHOTON IONIZATION IN CONICAL LASER BEAMS

Multiphoton ionization of xenon near three-photon atomic resonances has well been investigated for a wide range of excitation conditions [77 – 79, 83, 85 – 87, 99 – 101, 103 – 105]. As an example, Fig. 4 shows the REMPI spectrum of xenon in the spectral region 430 – 446 nm. This spectrum was measured with the use of an ordinary Gaussian beam, when the dye laser beam was focused into the cell by a lens  $f = 75$  mm. REMPI spectrum demonstrates a number of atomic resonances of xenon. These resonances arise due to the four-photon excitation of intermediate  $4f$  and  $8p$  atomic states of xenon with subsequent ionization by absorption of one laser photon (a 4+1 process in REMPI terminology). The wavelength 440.88 nm corresponds to the position of the three-photon  $6s$  resonance, but the corresponding atomic peak in spectrum is absent. It is a result of well-known destructive wave-mixing interference in three-photon resonant excitation of atomic transitions [77 – 79, 83, 87, 90, 99 – 101, 106, 107]. Briefly, when three-photon excitation of a dipole-allowed atomic transition is attempted at elevated concentrations, a coherent sum-frequency

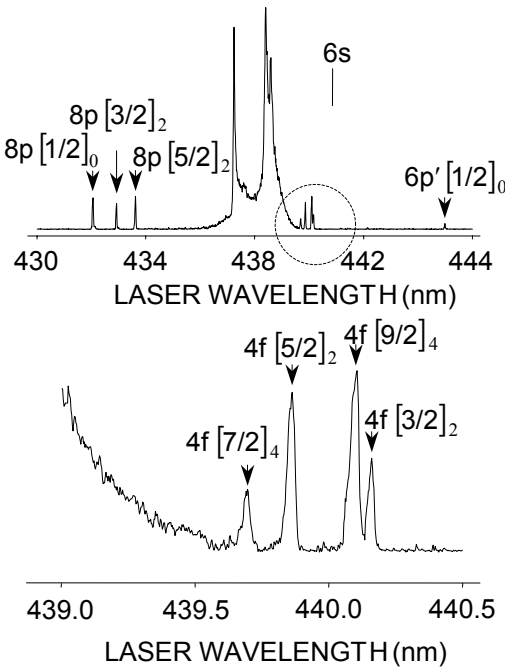


**Figure 4.** Wavelength scans of ionization signal near the  $6s$  resonance. Xenon pressure 1 bar.

field is generated at the resonant transition frequency. The overall transition amplitude becomes determined by two coherent processes – the three-photon excitation by the fundamental field and the one-photon excitation by sum-frequency field. In conditions of strong resonant absorptions of sum-frequency field these excitation pathways have equal amplitudes but opposite phases so that the two excitation pathways interfere destructively. As a result, no excitation of the atomic state occurs above some certain threshold product of number density and oscillator strength. In experiments on REMPI in rare gases these destructive interference leads to the well-known cancellation of

three-photon atomic resonances, which are diminished and disappear into background at an increased gas pressure. It is just the case for spectrum in Fig. 4. The canceled atomic resonances reappear in REMPI spectra in counter-propagating laser beams, when the wave-mixing interference is modified [79, 83, 87, 99 – 101]

With focused Gaussian beams, the phase-matched TH can be generated in the high-energy side of the  $6s$  resonance, where dispersion is negatively. Frequency tripling in this spectral region is a well-known and widely spread method for producing coherent VUV radiation near 147 nm [108 – 112]. With an increased gas pressure the peak of generated TH is moved rapidly toward shorter wavelength and no TH ionization peaks is registered with Gaussian beams near the resonance position at an elevated xenon pressure. Ionization spectra undergo significant changes when the laser beam is focused by an axicon instead of a spherical lens [113]. For a Bessel beam, a prominent ionization peak appears very close to the  $6s$  resonance whereas such band is absent for the ordinary Gaussian beams [113, 114]. This band is due to the generation of phase-matched TH and the difference of REMPI spectra reflects different excitation geometry of the Bessel and the Gaussian beams [113, 114]. In this section, the TH generation process in Bessel and other conical beams is considered.

## 4.1. Results and discussion

Two kinds of conical laser beams were used in experiments: a full-aperture Bessel beam and several segmented conical beams. The laser output was

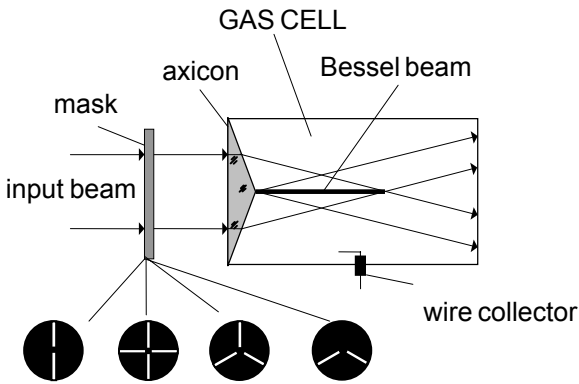


**Figure 5.** Schematic of experimental arrangement for REMPI measurements with conical laser beams.

focused into the gas cell by axicon (Fig. 5) and the produced Bessel beam had the inclination angle  $\alpha = 17^\circ$ . The light intensity in the excitation region was up to  $10^{10}$  W/cm<sup>2</sup>. Spatial distribution of light intensity in the focal region of this Bessel beam is shown in Fig. 6(a). With the aid of different masks, a part of the conical wave front was

blocked and the transformations of the TH excitation profiles were studied.

Figure 7(a) demonstrates the TH excitation profile for a full-aperture Bessel beam. The shape of this profile is known from earlier studies [33, 113, 114]. For moderate values of gas pressure, the profile has a well pronounced sharp

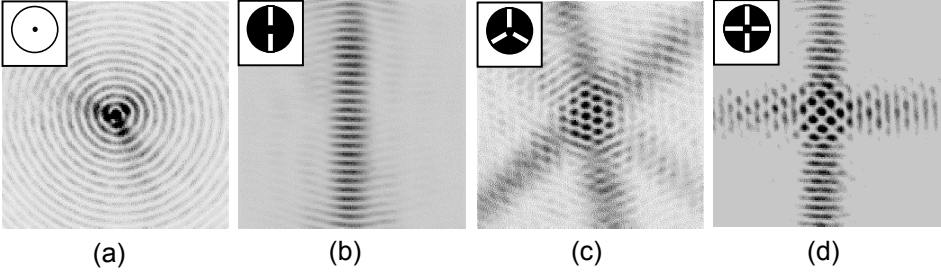


**Figure 6.** CCD-pictures of the focal regions: (a) full-aperture Bessel beam; (b)–(d) segmented conical beams. The insets show the used masks.

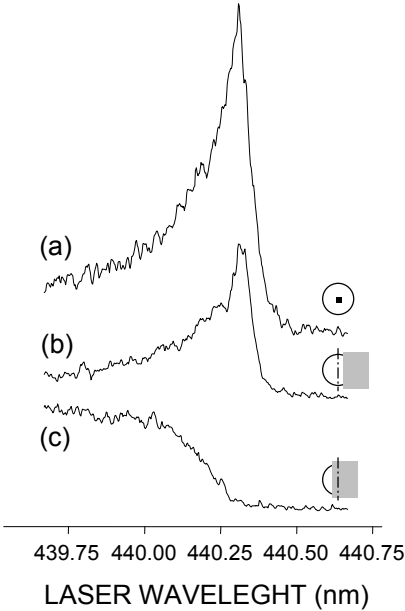


**Figure 7.** Ionization profiles resulting from modified beam profiles: (a) – full-aperture conical beam (Bessel beam); (b) – mask covers slightly less than half of the incident beam profile; (c) – mask covers slightly more than half of the incident beam (laser pulse energy was increased by 1.5 times).

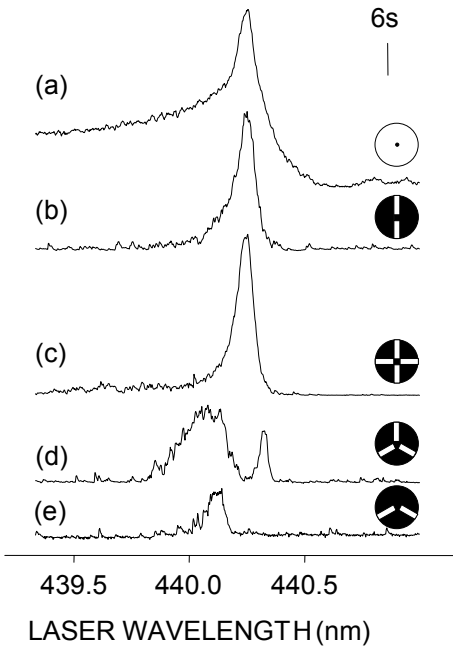
maximum followed by a tail toward the short-wavelength side and some, though much smaller, wing on the long-wavelength side. The position of the TH maximum shifts linearly to the shorter wavelength with increased gas pressure. This shift depends on the inclination angle of the Bessel beam and for  $\alpha = 17^\circ$  it was 0.32 nm/bar. Note, that for such relatively large inclination angle the phase-matched TH is generated close to the resonance position and the TH absorption is very strong [33, 96]. In this case, the TH emission from the gas cell is very weak but the TH generation process is easily monitored through ionization of the target gas.

Experiments with masked beams have shown that any distortion of the amplitude profile of the incident laser beam lead to significant and very specific transformations of the TH excitation band. Fig. 7 demonstrates transformation of the TH excitation profile at closing certain part of the incident laser beam. In experiment, the

mask was moved step-by-step into the incident laser beam starting from the completely open position. When mask blocked a part of the incident beam, distinct transformations of the TH profile occurred. Most pronounced was the suppression of the main TH peak, while the short-wavelength tail was much more tolerant against beam masking. Suppression of the maximum goes rather rapidly when the mask closes approximately a half of the beam. Fig. 7(b) shows the TH profile in position when the mask covered slightly less than a half of the incident beam. The maximum still is observed, but it is suppressed appreciably. At a further movement of the mask into the beam, the TH peak is reduced rapidly and disappears entirely when the mask covered slightly more than a half of the incident beam. By contrast, the tail of the TH band did not show any significant transformation and it was observable at any mask position.

In order to analyse the transformation of the TH profile in more detail, a set of various slit masks was used (Fig. 5). Slit masks were placed close to the entrance surface of the axicon. The width of slits was 0.6–0.8 mm. In all cases the central part of the axicon was blocked by a 1–1.5 mm obstacle. Slit masks selected some radial slices of the laser beam and these selected sub-

beams were focused by the axicon forming segmented conical beam where a large parts of the pump field components are blocked and the input source becomes comprised of sub-beams from a limited range of available azimuthal angles. As in the case of the full-aperture Bessel beam, all components of segmented beams remain inclined by the angle  $\alpha$  toward the propagation axis and crossed along this axis, but the TH excitation process is driven by selected spatial configuration of pump field. Spatial distribution of light intensity in some segmented beams is shown in Fig. 6(b–d).



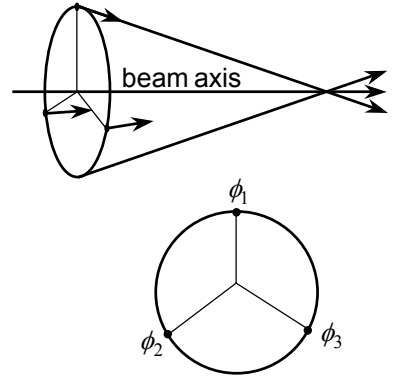
**Figure 8.** Transformation of the TH ionization profiles with the use of slit masks: (a) – full-aperture Bessel beam; (b–e) – segmented conical beams. Xenon pressure 2 bar.

Figure 8 shows an example of experimental results with slit masks. Again, the TH excitation profile for the full-aperture Bessel beam (no mask) is shown (Fig. 8(a)). With the use of a linear-slit mask (Fig. 8(b)) the TH

profile is squeezed to a single Lorentzian-like peak at the position of the TH maximum in the initial unmasked Bessel beam. For other masks additional spectral components can be recognized in the spectra. For two crossed slits (Fig. 8(c)), the same peak was registered together with an additional weak band on the short-wavelength side. For the mask with three slits separated by  $120^\circ$  (Fig. 8(d)), the TH profile again has two components – a sharp Lorentzian-like peak and a short-wavelength band. The peak in this case is located closer to the  $6s$  resonance than the peak for one- or two-slit masks. When any one of the three  $120^\circ$  slits was blocked, the peak disappeared and only the broad short-wavelength band remained in the profile (Fig. 8(e)).

To analyze the TH excitation profiles in segmented beams, consider first the origin of different spectral components of these profiles. In the description of a wave-mixing process from a full-aperture Bessel beam, all combinations of particular waves having any azimuthal angle  $\phi_i$  from  $0^\circ$  to  $360^\circ$  on the light cone are superimposed (Fig. 9). In segmented beams some of such combinations disappear. For the TH generation process, two principal geometries of interacting sub-beams should be considered. The first is the general case of photons from each of three interacting fundamental plane waves having different azimuthal angles  $\phi_1$ ,  $\phi_2$ , and  $\phi_3$ . The second is the two-beam case, where two fundamental photons come with the same azimuthal angles

$\phi_1 = \phi_2$  and the third photon comes from another part of the light cone ( $\phi_3 \neq \phi_1$ ). The collinear (single beam) case  $\phi_1 = \phi_2 = \phi_3$  is excluded since no phase-matched TH is produced by a single plane wave for the spectral range of interest. For each elementary two- or three-beam combination, the excitation problem is reduced to the well-known process of the TH generation in two or three crossed plane waves. In conditions of strong TH absorption this task is much simplified since the TH excitation profile becomes a Lorentzian [115 – 118]. This Lorentzian arises on the short-wavelength wing of the atomic line and the width of this TH peak is equal to the width of pressure-broadened atomic line. The shift of the Lorentzian profile from the atomic resonance depends on crossing angle between the pumping waves and the gas pressure [115 – 119]. The appearance of such Lorentzian ionization profile displaced



**Figure 9.** Noncollinear interaction of three fundamental waves with different azimuthal angles  $\phi_1$ ,  $\phi_2$ , and  $\phi_3$  in conical light beams.

from the resonance position can be treated in terms of the so-called cooperative line shift [117 – 120]. In [114] it was shown that at any gas pressure, the location of the peak of the pressure-dependent ionization profile in a Bessel beam with inclination angle  $\alpha$  matches exactly the value of the cooperative shift for two plane waves crossed at angle  $2\alpha$ . In other words, the peak of the TH profile in a Bessel beam corresponds to the peak of the atomic line shifted by the cooperative shift of the resonant frequency under noncollinear excitation.

With linear-slit mask, selected is an elementary two-beam configuration of beam components. This two sub-beams are entering the excitation zone from the opposite sides of the light cone and the TH generation proceeds via a planar combination of two interacting sub-beams, where two fundamental photons are taken from one sub-beam and the third photon comes from another sub-beam from the opposite side ( $\phi_1 = \phi_2$  and  $\phi_3 = \phi_1 + 180^\circ$ ). Fig. 8(b) shows that for such linear-slit mask a Lorentzian-like peak appears at the position of the TH maximum in the Bessel beam of Fig. 8(a) exactly as expected.

For two crossed slits (Fig. 8(c)), the same Lorentzian peak was observed together with an additional weak band on the blue side of the main peak. In this case, there are three possible combinations of sub-beams. The first combination is realized for each set of two slits similar to the case of linear slit geometry. These combinations produce the same Lorentzian peak as in Fig. 8(b). In a second possible combination, two photons come from the opposite sides of a slit and the third photon comes from another slit ( $\phi_2 = \phi_1 + 180^\circ$ ,  $\phi_3 = \phi_1 + 90^\circ$ ). As it was shown in [114], such non-planar three-beam combination is equivalent to a planar two-beam combination giving the main TH peak. The last is a two-beam combination, where two photons come from one side of a slit and third photon comes from another slit ( $\phi_1 = \phi_2$ ,  $\phi_3 = \phi_1 \pm 90^\circ$ ). This particular combination is responsible for the appearance of the weak TH band to the blue of the main peak.

For two crossed unfocused beams, the location of the pure Lorentzian component in the spectrum is determined by the applicable value of the cooperative frequency shift  $\delta_c$  given by [117 – 120]

$$\delta_c = \Delta_0 \left[ -1.11 + \frac{9}{1 - \cos \theta} \right] = \frac{9\Delta_0}{2 \sin^2 \theta/2}, \quad (5)$$

where  $\Delta_0 = \pi N F_{01} e^2 / 2m\omega_0$ ,  $N$  is the gas density,  $F_{01}$  is the oscillator strength,  $\omega_0$  is the resonance angular frequency, and  $\theta$  is the angle between two waves. In the present context the small term  $-1.11\Delta_0$  can be omitted in the

following considerations. It is easy to see that two particular waves with azimuthal angles  $\phi_1$  and  $\phi_2$  on the light cone will cross at an angle  $\theta$  given by

$$\sin \frac{\theta}{2} = \sin \frac{\phi}{2} \sin \alpha, \quad (6)$$

where  $\phi = \phi_2 - \phi_1$ . Using this expression, Eq. (5) can be written as

$$\delta_c = \frac{9\Delta_0}{2\sin^2(\frac{\theta}{2})} = \frac{9\Delta_0}{2\sin^2 \frac{\phi}{2} \sin^2 \alpha} = \frac{\delta_0}{\sin^2 \frac{\phi}{2}}, \quad (7)$$

where  $\delta_0 = 9\Delta_0/2\sin^2 \alpha$  determines the position of the main peak with  $\theta = 2\alpha$ . Thus, the shifted position of the Lorentzian peak for any given pair of sub-beams can be determined in units of  $\delta_0$ . It is illustrated in Fig. 10, where some experimental profiles are shown together with the calculated locations of

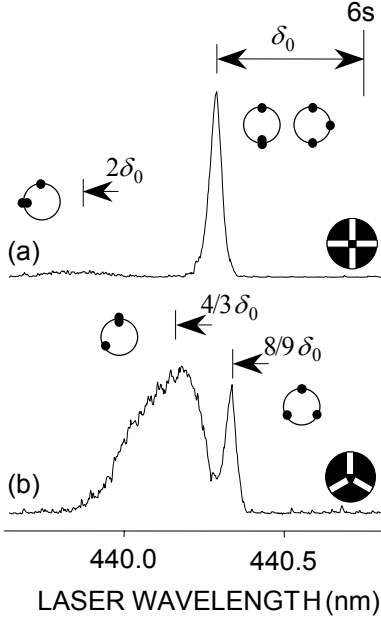


**Figure 10.** Comparison of experimental TH profiles and calculated positions of the TH components for different sub-beam combinations. Xenon pressure 2 bar.

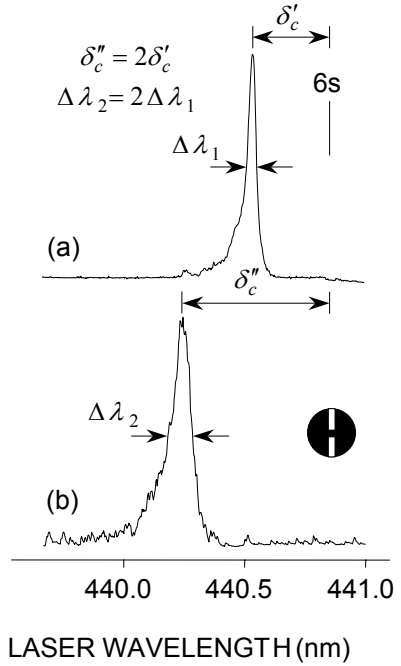


**Figure 11.** Evolution of the TH profile (cooperative line) with xenon pressure: (a) – 1 bar; (b) – 2 bar.



the TH components for different sub-beam combinations. For two beams crossing at  $\phi = 90^\circ$  the shift is  $\delta_c = 2\delta_0$  (Fig. 10(a)). This point corresponds exactly to the maximum of the blue band registered with two crossed perpendicular slits (Fig. 10(a), Fig. 8(c)). Similarly, for  $\phi = 120^\circ$  the shift is  $\delta_c = 4/3\delta_0$ . Again, this point can be recognized in spectra as the maximum of the band registered with two or three slits separated by  $120^\circ$  (Fig. 10(b), Fig. 8(d, e)).

The width and the location of all TH components in spectra depend on xenon pressure. It is illustrated in Fig. 11 for the beam segmented by a linear-slit mask. The top and the bottom traces show the Lorentzian-like TH peak at the pressure of 1 bar and 2 bar, respectively. The width of the peak is proportional to xenon pressure (35 pm/bar FWHM in terms of the laser wavelength) and matches exactly the theoretical value for the pressure-induced width of the atomic 6s resonance of xenon [121]. The shift  $\delta_c$  of the peak from the 6s resonance is also linear with pressure. This shift depends on the inclination angle of the initial Bessel beam and for the case here it was 0.32 nm/bar.

For any two-beam combination, the TH profile should have a Lorentzian shape with the width independent of crossing angle. However, the spectral profiles produced by sub-beams crossing at  $90^\circ$  and  $120^\circ$  were registered as broad bands instead of narrow Lorentzians (Fig. 8, Fig. 10). This effect results from the angular spreading of individual sub-beams, since the finite width of mask slits and diffraction on mask edges give some spreading in angles  $\phi_i$ . This spreading is maximum for the inner edges of the slits and in the present case it was up to  $\pm 20^\circ$ .

The sensitivity of  $\delta_c$  to the angular spreading  $d\phi$  can be estimated by  $d(\delta_c)/d\phi$  as

$$d(\delta_c) = -\frac{\delta_0}{\sin^2 \frac{\phi}{2} \tan \frac{\phi}{2}} d\phi = -\frac{\delta_c}{\tan \frac{\phi}{2}} d\phi. \quad (8)$$

This expression shows that the larger is the value of  $\phi$ , the less sensitive is  $d(\delta_c)$  to  $d\phi$ , and that  $d(\delta_c) \rightarrow 0$  at  $\phi \rightarrow 180^\circ$ . For the pure Lorentzian peak produced from a linear-slit geometry, where  $\delta_c = \delta_0$ , the angular spreading of  $\pm 20^\circ$  leads to a negligible (about 5%) broadening of this peak. By contrast, for beams crossing at  $120^\circ$  the same spreading leads to an asymmetric broadening of the corresponding Lorentzian by  $0.2\delta_0$  to the red and by  $0.37\delta_0$  to the blue. For beams crossing at  $90^\circ$  the broadening is further increased, being about  $0.5\delta_0$  and  $\delta_0$  for the red and the blue sides, respectively. As a result, instead of

narrow Lorentzians, broader bands were registered for crossing angles  $90^\circ$  and  $120^\circ$ .

For the general case of three nonplanar interacting waves from the axicon, the cooperative shift is given by expression [38]

$$\delta_c = \frac{18\Delta_0}{\sin^2 \alpha [3 - \cos(\phi_1 - \phi_2) - \cos(\phi_1 - \phi_3) - \cos(\phi_2 - \phi_3)]}, \quad (9)$$

or, assuming  $\phi_1 = 0$

$$\delta_c = \frac{4\delta_0}{3 - \cos \phi_2 - \cos \phi_3 - \cos(\phi_2 - \phi_3)}. \quad (10)$$

For three beams separated by  $120^\circ$  this expression gives the value  $\delta_c = 8/9 \delta_0$  for the shift. Among all possible two- and three-beam combinations from segmented conical beams, this is the minimum value of the cooperative shift. The corresponding peak was registered in experiments with the three-slit mask (Fig. 10(b), Fig. 8(d)). As expected, this peak had a Lorentzian profile with the same width of 35 pm/bar FWHM. It should be noted that for this symmetrical three-beam configuration the generated TH field is directed along the axis of the fundamental conical beam. For such a case, the general expression for the TH generation in Bessel beams [30, 31] gives zero TH intensity. However, experiments with segmented conical beams have shown remarkable TH production for such symmetrical configuration. In full-aperture Bessel beams the contribution from this particular combination gives a discernible broadening of the red wing of the main TH peak.

The sensitivity of the three-beam  $\delta_c$  to the angular spreading  $d\phi$  can again be estimated by  $d(\delta_c)/d\phi$ :

$$d(\delta_c) = -\frac{4\delta_0[(\sin \phi_2 + \sin(\phi_2 - \phi_3))d\phi_2 + (\sin \phi_3 - \sin(\phi_2 - \phi_3))d\phi_3]}{[3 - \cos \phi_2 - \cos \phi_3 - \cos(\phi_2 - \phi_3)]^2}. \quad (11)$$

For symmetric three-beam configuration  $d(\delta_c) \rightarrow 0$  when  $\phi_2 \rightarrow 120^\circ$  and  $\phi_3 \rightarrow 240^\circ$ . In the present case of  $\pm 20^\circ$  spreading, the corresponding Lorentzian peak gets only a minor (about 5%) broadening toward shorter wavelength.

For a full-aperture conical beam there is an infinite number of pairs of interacting waves having different crossing angles and, thus, different values of the cooperative shift. This leads to large spreading of individual Lorentzians in

the full Bessel-beam spectrum. The overall TH envelope for a Bessel beam builds up as a superposition of such Lorentzians. This superposition of shifted lines has an interesting formal similarity with inhomogeneous broadening of spectral response in a system where individual homogeneous components get spectral spreading (e.g. due to Doppler effect) and superposition of these components produces the overall inhomogeneous spectral profile. With this analogy, the whole TH profile for a Bessel beam can be viewed as the result of “beam-geometry broadening” of the cooperative line, analogous to inhomogeneous broadening of an atomic line profile. This broadening arises due to an infinite number of possible combinations of interacting waves in Bessel beams, when every particular combination gives its own “homogeneous” contribution to the resulting excitation profile. Segmentation changes the Bessel-beam profile, as some combinations of the fundamental waves are blocked and the corresponding parts of the TH profile disappear. This situation is in some sense analogous to the “hole burning” in an inhomogeneous spectral profile. Here one can extract a selected “homogeneous” component from the profile of superimposed Lorentzians (Fig. 12). Because of axial symmetry of a full-aperture conical beam, it is impossible to form a “homogeneous dip” in the TH profile, as none of the masks is able to block all spatial configurations of a given geometry. Nevertheless, for conical beams it is possible to separate some single configurations while blocking all others. In this case, the overall ionization profile is reduced to a single “homogeneous” spectral component (Fig. 8(b)).

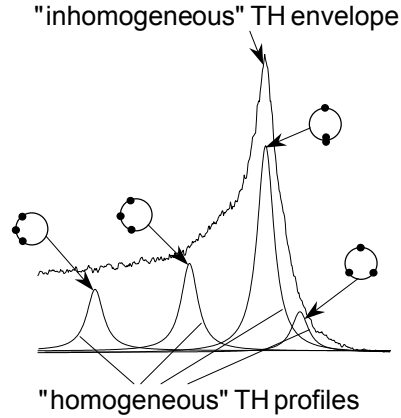


**Figure 12.** Some “homogeneous” Lorentzian components produced by elementary configurations of the fundamental field in the “inhomogeneous” TH envelope of a full-aperture Bessel beam.

## 4.2. Numerical simulation of the TH profiles

In description of the TH generation process in a full-aperture Bessel beam, all combinations of partial waves having any azimuth angle  $\phi$  from  $0^\circ$  to  $360^\circ$  on the light cone are superimposed. For every configuration of two or three crossing plane waves the concept of the cooperative line shift predicts the

excitation (ionization) profile as a Lorentzian peak. The excitation signal from the TH generation depends also on the interaction length of pumping sub-beams (gain length) and the overall excitation volume. In a Bessel beam, the light is concentrated along the propagation axis forming beam-like region with maximum light intensity. Any nonlinear process driven by a Bessel beam is confined to this narrow and extended core near the beam axis. If  $d$  is the diameter of the central lobe of a Bessel beam, the interaction length  $L = d / \sin \alpha$  is the same for any sub-beam combination since all sub-beams of the fundamental field have the same inclination angle  $\alpha$ . The propagation distance of the TH light in optically thick medium is very short and all the generated TH photons are absorbed entirely within the excitation region. It means that the same excitation volume for all sub-beam combinations can be assumed. Thus, to evaluate the TH production in a Bessel beam one can use simple picture of equally weighted Lorentzians, where any partial combination of the fundamental sub-beams yields the same “brightness” of the corresponding TH peak. These Lorentzians are variously displaced by the cooperative shift, but all of them have equal amplitudes. In segmented and Mathieu beams the intensity profile differs significantly from the Bessel pattern (Fig. 6). In this case, the approach of equally-weighted Lorentzians may not be valid since the gain length and/or the excitation volume can be different for different sub-beams combinations.

For the general case of three interacting waves from a conical wave front, the location of the cooperative line is given by Eq. (9) for the cooperative shift  $\delta_c$ , where the angles  $\phi_i$  have all possible choices from  $0^\circ$  to  $360^\circ$ . For the case here, Eq. (9) can be written as

$$\delta_c = \frac{4\delta_0}{3 - \cos(\phi_1 - \phi_2) - \cos(\phi_1 - \phi_3) - \cos(\phi_2 - \phi_3)}, \quad (12)$$

where  $\delta_0$  determines the position of the main TH peak. For the general case of three sub-beams, the inclination angle  $\beta$  of the TH wave vector is given by

$$\tan \beta = \frac{1}{3} (\tan \alpha) \sqrt{3 + 2(\cos(\phi_1 - \phi_2) + \cos(\phi_1 - \phi_3) + \cos(\phi_2 - \phi_3))}. \quad (13)$$

Thus, Eq. (12) can be written as

$$\delta_c = \frac{8\delta_0}{9 \left( 1 - \frac{\tan^2 \beta}{\tan^2 \alpha} \right)}. \quad (14)$$

Equation (14) couples the spectral variable  $\delta_c$  and the angular variable  $\beta$ . The angle  $\beta$  changes from 0 to  $\alpha$  when  $\delta_c$  changes from its minimum value of  $\delta_c = 8/9\delta_0$  to infinity.

The overall TH excitation profile in a Bessel beam builds up from all elementary TH components. This profile is to be found as a squared sum of all partial TH amplitudes. In conditions of strong TH absorption, however, all generated TH photons are absorbed within the excitation volume. One can suppose that the integral excitation characteristics in such conditions can be found as a simple incoherent sum of intensities rather than a coherent sum of amplitudes [122].

Every particular TH profile, monitored in an optically thick medium through atomic excitation and subsequent ionization, is a Lorentzian cooperative line with a pressure-dependent width  $\Gamma$  (FWHM) and the cooperative shift  $\delta_c$ . For an excitation frequency  $\omega$ , the contribution of any elementary sub-beam configuration into the overall excitation envelope is thus given by:

$$I(\omega) = \frac{\Gamma/2\pi}{(\omega - \omega_0 - \delta_c)^2 + \frac{\Gamma^2}{4}}, \quad (15)$$

where  $\omega_0$  is the resonance frequency,  $\omega_0 + \delta_c$  is the central frequency of a Lorentzian line, and  $\delta_c$  is given by Eq. (12). Cylindrical symmetry of the Bessel beam allows one to fix  $\phi_1 = 0$  and the overall signal  $S(\omega)$  from the TH generation is then given by integral over azimuth angles  $\phi_2$  and  $\phi_3$ :

$$S(\omega) = \int_0^{2\pi} \int_0^{2\pi} I(\omega, \delta_c(\phi_2, \phi_3)) d\phi_2 d\phi_3. \quad (16)$$

Figure 13 shows the TH excitation profile calculated using Eq. (16) for  $\delta_0 = 18\gamma$ . Such  $\delta_0$  corresponds to the experimental conditions of previous sub-section, where the Bessel beam with  $\alpha = 17^\circ$  was used to generate TH near the  $6s$  resonance of xenon. Calculated profile in Figs. 13 and 14 shows sharp near-resonance peak followed by a tail toward the short-wavelength side of the spectrum. Such shape of the TH excitation profile is in very good agreement with the TH bands registered in low-pressure ionization experiments [33, 114]. For a high gas pressure, the experimental profiles (Fig. 14(b)) show similar shape but with less pronounced peak and a more intense tail because of additional molecular absorption in a dense gas. In agreement with experimental data, the location of the TH peak coincides the location of the cooperative line at  $\delta_0$  (curve (b) in Fig. 13). Long-wavelength wing of the TH band covers the region toward and beyond the resonance position at  $\omega_0$ . Again, it agrees very

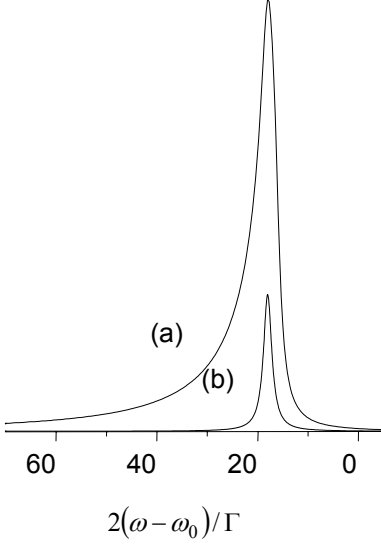


**Figure 13.** Numerical simulation of near-resonance excitation profiles associated with the phase-matched TH in an optically thick medium: (a) superposition of multiple Lorentzians in a Bessel beam; (b) single Lorentzian peak (not scaled to (a)) located at  $\delta_0$ .

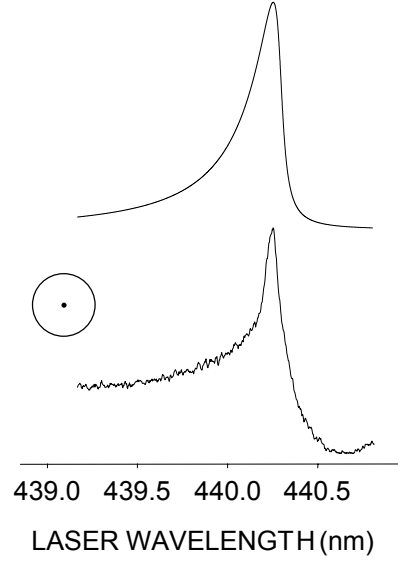


**Figure 14.** TH excitation profiles for a full-aperture Bessel beam  $\alpha = 17^\circ$ : top—numerical simulation; bottom—experiment. Xenon pressure 2 bar.

well with experimental observations [33, 113, 114]. The peak of the TH profile occurs at a wavelength where  $\delta_c = \delta_0$  and the angle  $\beta$  satisfies the well-known condition [30, 31] written as Eq. (4). In the case here, Eq. (4) follows from Eq. (14) at  $\delta_c = \delta_0$ .

Segmented and Mathieu beams share the propagation properties of a Bessel beam, but their amplitude profiles differ significantly from the Bessel pattern. Thus, for such beams the representation of the fundamental and the TH fields as Bessel beams is not valid. In segmented and Mathieu beams the light energy propagates along a cone surface, but the light field is comprised of sub-beams from a limited range of azimuth angles [39, 41]. Thus, some sub-beam combinations and corresponding TH components of a full-aperture Bessel beam disappear in segmented and Mathieu beams. In this sense, a Bessel beam is simply a particular case of full-aperture conical excitation geometry when the azimuth angles  $\phi_i$  of sub-beams have any value from  $0^\circ$  to  $360^\circ$ . With the present approach, the source field of a non-Bessel conical field can again be decomposed into elementary sub-beam combinations and the overall TH excitation profile is then constructed from partial TH profiles. The general

formalism remains the same, except for a restriction of the azimuth angles to a limited extent.

Figure 15 shows the TH excitation profile calculated for a conical beam segmented by symmetrical three-slit mask. Such mask was used in experiments with segmented beams (see previous sub-section) and the experimental TH profile is also shown in Fig. 15. The calculated profile in Fig. 15 was obtained by numerical evaluation of the integral

$$S(\omega) = \int \int \int_{\phi_1 \phi_2 \phi_3} I(\omega, \delta_c) d\phi_1 d\phi_2 d\phi_3, \quad (17)$$

where  $I(\omega, \delta_c)$  is given by Eq. (15) and  $\delta_c$  is given by Eq. (12). Being segmented by a mask, the range of possible azimuth angles in conical beams is determined by two factors. First, this range is given by geometry of the used mask. For the case shown in Fig. 15, the mask selected three sub-beams separated by  $120^\circ$ . Second, a finite width of mask slits and diffraction on mask edges give some spreading  $\pm \Delta\phi$  of the azimuth angles for every selected sub-beam. Thus, for the case considered all the azimuth angles  $\phi_i$  in Eq. (17) run over three ranges of  $\pm \Delta\phi$ ,  $120^\circ \pm \Delta\phi$ , and  $240^\circ \pm \Delta\phi$ . Best calculation results were obtained for  $\Delta\phi = 15^\circ - 20^\circ$ , that agrees well with the value of spreading of up to  $\pm 20^\circ$  estimated in experiment.

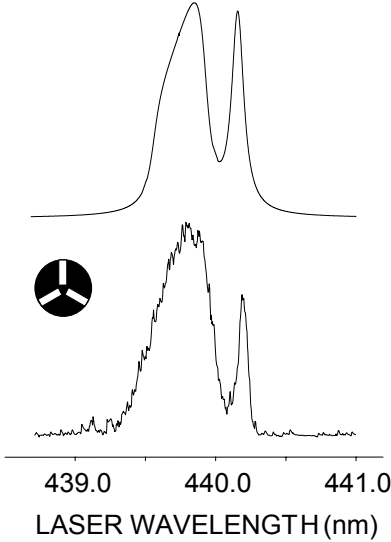


**Figure 15.** TH excitation profiles for segmented conical beam: top—numerical simulation; bottom – experiment. Xenon pressure 1 bar.

The TH profiles in Fig. 15 have two distinct spectral components. Sharp near-resonance peak results from three-beam excitation, when all three sub-beams enter the excitation zone from different slits. Spectral spreading of individual Lorentzians in this case is small and the envelope is formed as a sharp and narrow peak located at  $\delta_c = 8/9 \delta_0$ . If any pair of sub-beams enters the excitation zone from the same slit (two-beam excitation), the range of  $\delta_c$  is larger and individual Lorentzians are spread over a more broad spectral range. It yields a second component of the profile as a broad band located at the short-wavelength side of the peak. Finally, when all three sub-beams enter the excitation zone from the same slit (single-beam excitation), the range of shift is  $\delta_c > 15\delta_0$  and the

corresponding TH components are located off the range of interest. Such far wing of the TH envelope is very weak since the spectral density of Lorentzians is reduced rapidly with an increased  $\delta_c$ . Spectral density of elementary profiles is discussed in more detail below in sub-section 6.3.

Simulation of the TH profile in Fig. 15 was again based on the approach of equally-weighted Lorentzians. For the beam considered, such an assumption is correct since interaction length and excitation volume are nearly equal for all two- and three-beam combinations of the source field. For other segmented conical beams such an assumption may be incorrect. However, an accurate account for the gain length and the excitation volume will allow one to apply the present treatment of the problem to other beam configurations, as well.



## 5. SPATIALLY INCOHERENT LASER BEAMS

All conical beams considered above were characterized by a complete spatial coherence. Coherent laser beams are usually used in most studies and applications while incoherent beams are less common. Intense incoherent beams are able to induce a variety of nonlinear processes, but peculiarities of such processes are much less known. Therefore, the considered problem of sum-frequency generation and multiphoton ionization was initially studied in a reference excitation geometry, when incoherent beams were focused to the target gas by ordinary spherical optics. The results of this study give a natural basis for comparison of excitation processes in different conditions.

### 5.1. Experimental arrangement

Figure 16 shows two excitation geometries used in experiments with spherical optics. The dye laser was used as a source of coherent radiation and the excimer laser served as a source of incoherent UV radiation synchronized with the pulses of dye laser. The dye and UV laser beams were made copropagating with the aid of a quartz splitter. The splitter had a small wedge angle and reflected about 4% of the UV pulse from every surface. One of these reflected UV beams was blocked and the second, with typical energy of 50–100  $\mu\text{J}$ , was directed to the gas cell. In the collinear excitation mode, both the UV and the dye laser

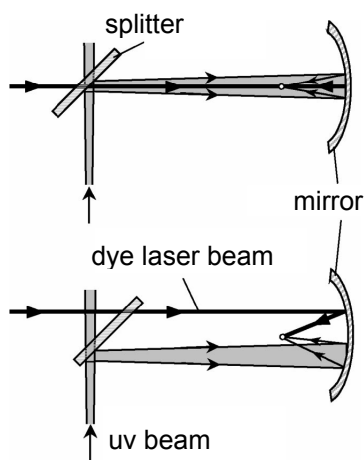


**Figure 16.** Geometry of the two-color excitation: top, collinear excitation; bottom, noncollinear excitation.

beams propagated along the same axis. These beams passed through the windows of the gas cell and were focused back into the cell by an on-axis spherical mirror of focal length  $f = 30$  mm. The use of mirror avoided chromatic aberrations. The same optical arrangement was used in experiments with crossed beams. In this case, however, some distance between the beam axes was introduced and both beams were made propagating parallel. Focused by the mirror, beams crossed at the focal region. In this noncollinear excitation mode the aperture of the cell windows allowed one to get crossing angles up to  $20^\circ$ .

Divergence of the dye laser beam (full

angle  $2\theta$ ) was 0.5 mrad and exceeded the diffraction limit by 1.5 – 2 times only. It means a high degree of the beam spatial coherence. It was checked additionally with the use of a prism interferometer [123]. The initial beam was split into two sub-beams and one of these sub-beams was then rotated in its own plane by  $180^\circ$ . Being superimposed, sub-beams produced an interference pattern, which reflected mutual correlations of different parts of the wave front. The experiments have shown very good visibility of interference fringes, and thus a high degree of spatial coherence over the whole cross section of the dye laser beam.

Divergence of the UV beam from the XeCl laser was 2 – 2.5 mrad full angle and exceeded the diffraction limit by about two orders of magnitude. Such beam had a low degree of spatial coherence and contained multiple wave-front irregularities with the characteristic size of lateral correlations  $d_0 \sim \lambda/\theta \approx 0.3$  mm. The temporal coherence length of the excimer laser beam was measured with the aid of Michelson interferometer. This length was determined as the optical paths difference when the visibility of interference fringes was reduced to a half of maximum. The value obtained was  $1.0 \pm 0.2$  mm that corresponds to a bandwidth of about  $4 \text{ cm}^{-1}$  FWHM for a Gaussian spectral profile.

Different degree of spatial coherence for the dye and the UV beams resulted in their essentially different focusability. Fig. 17 shows the focal spots of beams measured by CCD camera in the focal region of a quartz lens. Because of

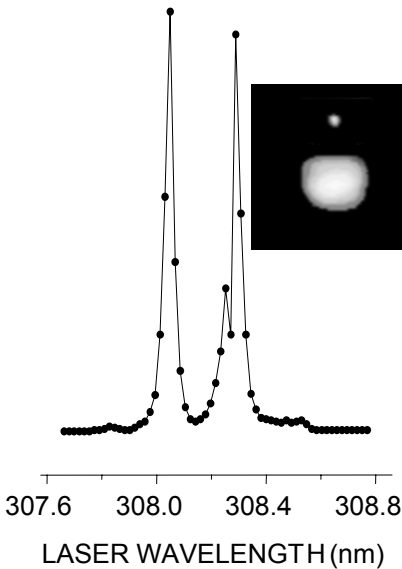


**Figure 17.** XeCl lasing spectrum and focal spots of the used dye and XeCl laser beams.

chromatic aberration, the minimum size of focal spots corresponded to slightly different focal distances. The size of spots was measured for different lenses having focal length from 450 mm to 100 mm and the results were extrapolated to the focal length  $f = 30$  mm of the mirror. Such extrapolation gave the size of about  $10 \mu\text{m}$  and about  $70 \mu\text{m}$  for the dye and the UV beam, respectively. Simple estimate of the focal spot diameter  $2w_0$  for incoherent beams  $2w_0 \approx (2\theta)f$  gives  $60 - 75 \mu\text{m}$  in good agreement with experimental finding. The confocal parameter  $b$  of the focused dye laser beam was about 0.3 mm. For the UV beam, an effective length  $b^*$  of the focal region can be estimated as  $b^* \sim 2w_0 / \theta_0 \approx 0.4$  mm,

where  $\theta_0 = D/2f$  is the focusing angle, and  $D \approx 10$  mm is the size of the UV beam on the mirror. Taking into account the losses on optical elements, the light intensity in the focal volume was about  $5 \times 10^7$  W/cm<sup>2</sup> for the UV pulse of 50  $\mu$ J and about  $5 \times 10^{10}$  W/cm<sup>2</sup> for the dye laser pulse of 1 mJ.

According to Van Cittert-Zernike theorem [94, 124], the ratio of the correlation radius  $r_c$  to the beam size remains unchanged under propagation. It means that in tightly focused incoherent beams the wave-front correlations can be squeezed in transverse directions to the size of a few wavelengths. These lateral local correlations decay after passing some distance along the propagation axis. The length of such correlated propagation is described by longitudinal spatial coherence function [125 – 129]. For a focusing angle  $2\theta_0 = D/f$  the characteristic size of transverse  $d$  and longitudinal  $\Delta z$  correlations in the focal region can be estimated as  $d = 2r_c \approx 2\lambda/(2\theta_0) \approx 2$   $\mu$ m and  $\Delta z \approx 4\lambda/(2\theta_0)^2 \approx 10$   $\mu$ m. Thus, the overall excitation volume of the UV beam can be considered as a set of multiple mutually uncorrelated spatial regions or coherent domains, where some degree of correlation is maintained. Within these domains, the field components may have all possible propagation directions within a cone of characteristic angular spread  $\theta_0$ . The pattern of coherent domains behaves like a transient speckled field, where correlation within a domain (or a transient speckle) is maintained during some time  $t \sim \tau_c$ , where  $\tau_c$  is the temporal coherence time.

Figure 17 shows the lasing spectrum of the used XeCl laser. This spectrum was measured with a 1-m double monochromator operated in the third order of a grating 1200 lines/mm. Two intense lines in the spectrum correspond to vibronic transitions  $0 \rightarrow 1$  and  $0 \rightarrow 2$  of the  $\text{XeCl}^*$  molecules [130, 131]. Two other lasing transitions  $0 \rightarrow 0$  and  $0 \rightarrow 3$  are much weaker. Main laser lines are separated by 0.24 nm or  $25$  cm<sup>-1</sup> and have the width of about 40 pm FWHM. The dip in one emission line is due to absorption by OH radicals in XeCl laser active medium [132]. The overall width of the lasing spectrum is about  $30$  cm<sup>-1</sup> and it corresponds to the coherence time of  $\tau_c \sim 10^{-12}$  s and the temporal coherence length  $l_c \sim 0.1$  mm. Note that in the focal region  $\Delta z \ll l_c$ . The temporal coherence length of the dye laser beam was 10 – 12 mm.

The two-color excitation and subsequent ionization of the target gas occurs in the focal region of the overlapped dye laser and UV beams. The presence of small-scale transient domains in the UV field restricts the distance of coherent interaction of both beams to the mean size of these domains. The length of coherent interaction depends on crossing angle since UV domains are extended along the UV beam axis. This length is maximum for copropagating beams and it is minimum for beams crossed at a right angle. In present experiments, the

beams had crossing angles up to  $20^\circ$  and the overall excitation volume, given by the focal volume of the dye laser beam, contained an order of  $10^3$  domains from the UV field.

## 5.2. Four-wave mixing in spatially incoherent laser beams

The lowest states of xenon accessible for three-photon excitation by linearly polarized light are the  $6s$  and the  $6s'$  states. Since one laser source is fixed near 308 nm, the corresponding three-photon transitions  $2\omega_{L1} + \omega_{L2}$  is induced at the dye laser wavelength near 447 nm for the  $6s'$  state and near 562 nm for the  $6s$  state. Excited  $6s$  atoms are ionized through absorption of either one UV or two dye laser photons. Excited  $6s'$  atoms are ionized by absorption of one photon from UV or dye laser beams. Under two-color excitation near the  $6s$  resonance, a group of  $nd$  resonances of xenon is excited by the dye laser beam alone and these resonance ionization peaks distort the excitation profiles of sum-frequency field [102]. Therefore, a detailed study of three-photon resonance excitation was carried out for the  $6s'$  resonance, where the corresponding spectral region was free of additional ionization features. Fig. 18 shows the REMPI spectra measured near the  $6s'$  resonance. The dye laser beam alone produced several ionization peaks due to the four-photon excitation of  $6p'$  atomic state of xenon (bottom trace in Fig. 18). With the UV beam added, an intense ionization band appears. This ionization band is due to the three-photon resonant excitation  $2\omega_{L1} + \omega_{L2}$  as expected. The ionization band has a distinct doublet structure with peaks separated by 0.25 nm near 447 nm. This spectral distance corresponds to  $12.5 \text{ cm}^{-1}$  and this is exactly one half of the  $25 \text{ cm}^{-1}$  separations of the peaks in the XeCl lasing spectrum. The location of the three-photon  $6s'$  resonance

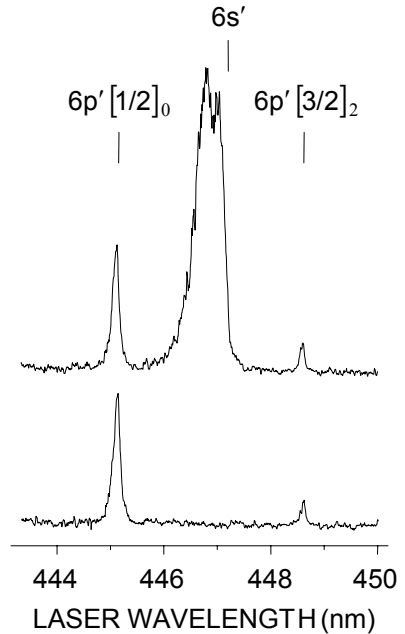


**Figure 18.** Wavelength scans of ionization signal near 447 nm: bottom, one-color excitation by dye laser beam; top, two-color excitation with UV beam added. Collinear excitation; xenon pressure 50 mbar.

marked in Fig. 18 correspond to the line  $\lambda = 308$  nm in the XeCl laser spectrum.

Figure 19 shows the evolution of ionization profiles with pressure in collinear excitation geometry. At a low gas density, the ionization profile has two well-separated peaks, which correspond to two emission lines in the UV beam. With an increased pressure, these peaks are broadened rapidly and overlap. Above 50 mbar the doublet structure of the band becomes unresolved and the ionization profile is registered as a single broad band. Broadening of profile components is followed by a distinct shift of the peaks from the resonance position toward

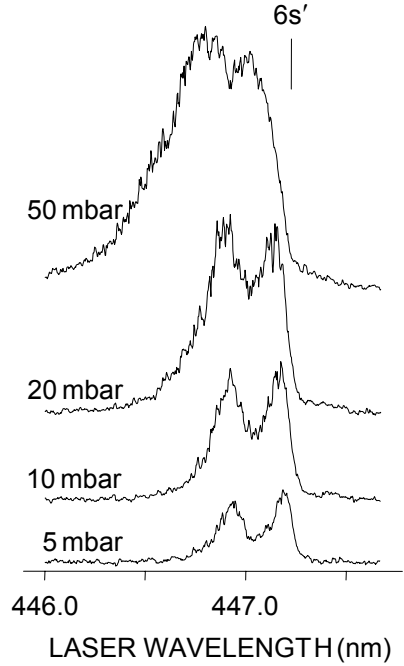


**Figure 19.** Evolution of the ionization band with pressure in collinear beams.

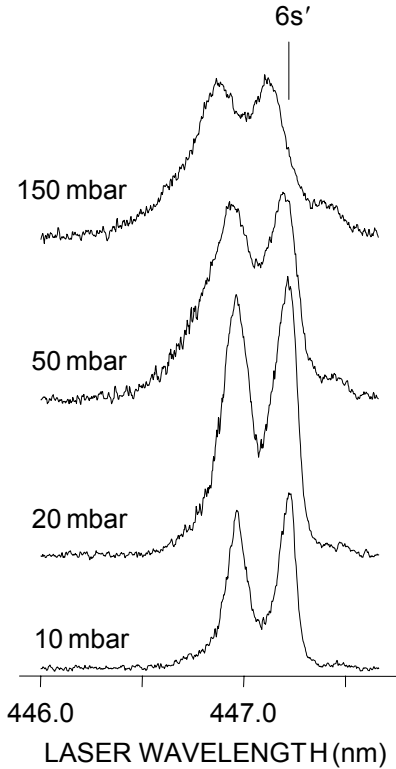


**Figure 20.** Evolution of the ionization band with pressure in crossed beams. Crossing angle  $\alpha = 18^\circ$ .

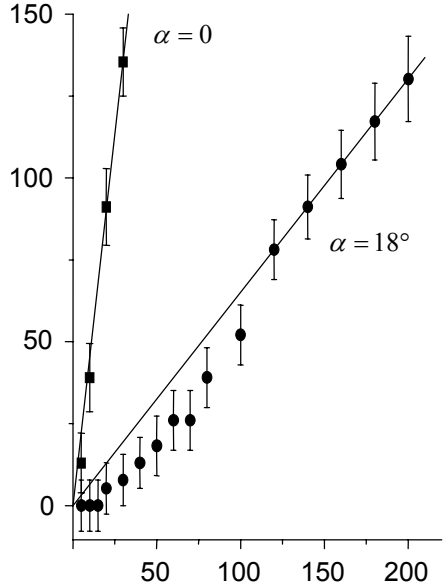
a shorter wavelength. Such an evolution of ionization profiles with pressure is a distinct indication for an excitation process where internally generated sum-frequency field dominates the resonant excitation [115 – 119]. Note that for collinear two-color excitation by coherent unfocused beams no resonance excitation is expected in a dense gas [117 – 119, 133]. In this case, the resonance peak is canceled and no phase-matched sum-frequency field is produced in the vicinity of the resonance.

Figure 20 shows pressure-dependent ionization profiles under non-collinear excitation by beams angled by  $18^\circ$ . For pressures below 20 mbar

no measurable changes in location and width of the peaks could be detected. The minimum width of peaks was  $0.1 \text{ nm}$  that corresponds to  $10 \text{ cm}^{-1}$  in two-photon scale. Compared with the width of  $4 \text{ cm}^{-1}$  for the UV laser lines, a significant contribution to the width of ionization peaks from the ac Stark effect can be stated. For three-photon pumping of the lowest  $6s$  resonance of xenon, the ac Stark shift constant of  $0.44 \text{ cm}^{-1} \text{ GW}^{-1} \text{ cm}^2$  was reported in Ref. [134]. For the case here, it means the magnitude of the ac Stark shift for the  $6s$  resonance of about  $20 \text{ cm}^{-1}$ . For the  $6s'$  resonance a similar ac Stark shift constant is expected. Thus, the broadening of the ionization peak should be of an order of  $10 \text{ cm}^{-1}$  in agreement with experimental observations. This broadening can be reduced through a decrease of the dye laser pulse energy. To keep the overall excitation probability, this decrease should be followed by an increase of the UV pulse energy. However, the UV light intensity had to be kept low since intense UV light produced strong parasitic ionization in the gas cell.

Above  $20 \text{ mbar}$ , a discernible broadening and blue shift of ionization peaks become evident. These shifts and broadening were much smaller than in collinear case and a doublet structure of the band could be detected at any gas pressure. Again, these transformations together with sensitivity to the crossing angle are distinct indications of the excitation process where sum-frequency field plays an important role.

Figure 21 shows plots of the shift of ionization peaks with pressure. For collinear beams, the shift and width of the ionization band were very sensitive to the shape of the UV beam and mutual alignment of UV and dye laser beams. The shift was linear with pressure and in different series of measurements a slope of  $3.5\text{--}8 \text{ nm/bar}$  was obtained. The dependence shown in Fig. 21 has the slope of  $4.5 \text{ nm/bar}$ . For noncollinear beams with a relatively large crossing angle, the sensitivity to the beam shape and adjustment was much weaker. In this case, sharp ionization peaks were well pronounced over the whole pressure range and the shift could be measured with a good accuracy. For crossing angle  $\alpha = 18^\circ$ , the shift



**Figure 21.** Pressure-induced shift of the ionization peaks.

becomes linear with the slope of 0.65 nm/bar above 100 mbar, but distinct deviations from this linear dependence were observed for the lower pressure range. The same behavior was observed in all other series of measurements with different crossing angles.

The shift of ionization peaks is linear with pressure and has distinct dependence on crossing angle. These observations follow exactly the well-known pattern of the three-photon-resonant excitation by crossed laser beams [115 – 119]. For two angled beams with different frequencies  $\omega_{L1}$  and  $\omega_{L2}$  the shift of the ionization profile from the resonance position is given by [117 – 119]

$$\Delta_c = \Delta_0 \left[ \frac{\lambda_{L1} + 2\lambda_{L2}}{\lambda_{mix}(1 - \cos \alpha)} \right], \quad (18)$$

where  $\Delta_0$  is given by Eq. 5 and  $\lambda_{mix} = 2\pi c / (2\omega_{L1} + \omega_{L2})$ . Parameter  $\Delta_0$  and the width  $\Gamma$  of pressure-broadened atomic line are coupled as  $\Gamma = 4.66\Delta_0$  [135]. For the  $6s'$  resonance of xenon, the values of  $\Gamma/N$  and  $\Delta_0/N$  are  $3.2 \text{ cm}^{-1}/\text{bar}$  and  $0.7 \text{ cm}^{-1}/\text{bar}$ , respectively. The shift  $\Delta_c$  is minimum at  $\alpha = 180^\circ$  and is directly proportional to gas pressure. When crossing angle is decreased the shift  $\Delta_c$  becomes very large and starting from some minimum angle  $\theta_{min}$  the ionization signal is decreased rapidly. In high-pressure xenon  $\theta_{min}$  is about  $0.1 \text{ rad}$  [119]. For  $\alpha > \theta_{min}$ , the ionization peak has the appearance of pressure-broadened atomic line, i.e., it has the amplitude and shape close to the corresponding pressure-broadened atomic line.

For collinear two-color excitation  $\alpha = 0$  and no ionization is produced at the atomic resonance since the excitation pathway through the atomic resonance is canceled and no phase-matched sum-frequency field is generated near the resonance. It is a well-known observation in experiments on collinear two-color resonant ionization in dense gases [117, 133]. However, the laser sources in Refs. [117, 133] had a high degree of spatial coherence as a common feature of narrow-band excimer-pumped dye lasers. Such regular coherent beams maintain the collinearity condition  $\alpha \approx 0$  over the whole interaction region. In the present case, one of the interacting light fields had poor wave-front coherence and the excitation region was irregular with multiple coherent domains. The angular spectrum of the incoherent light field determines some range of different propagation directions of field components and an essential local noncollinearity persists even for a collinear propagation of coherent and incoherent beams. According to Eq. (18) the slope of 4.5 nm/bar for collinear excitation (Fig. 21) corresponds to the crossing angle  $\alpha \approx 9^\circ$ , which is very close to the focusing angle  $\theta_0 \approx 10^\circ$  of the UV beam. For beams angled by

$\alpha = 18^\circ$  the slope was 0.65 nm/bar (Fig. 21). Formally, such a slope corresponds to the crossing angle  $\alpha \approx 24^\circ$ .

### 5.3. Analysis of spectral profiles

In order to analyze excitation profiles in incoherent beams, the concept of cooperative line shift (see previous section) together with simple geometrical consideration were used. The incoherent beam was considered as a set of small coherent domains having cylindrical symmetry and extended along the propagation axis  $z$  (Fig. 22). The angular spectrum of the incoherent field determines some range of crossing angles for the field components. All these components were assumed to have equal amplitudes with uniform distribution within a range of angles from zero to maximum angle  $\theta_0$ . In  $k$  space, such

an approximation makes the wave vectors  $\mathbf{k}_{L2}$  be distributed uniformly along all possible directions inside a cone with half-angle  $\theta_0$ . The coherent wave enters as a Gaussian beam, but for small-scale domains the length of the coherent four-wave interaction  $\Delta z$  is much smaller than the confocal parameter  $b$  of the focused Gaussian beam. Besides, transient intensity spikes in a multimode dye laser pulse have duration of  $10^{-10} - 10^{-11}$  s and such intensity changes are slow in the time scale of  $\Delta z/c$ . Thus, within a UV domain one can neglect all changes (associated with either focusing or spiking) of the dye laser beam in amplitude and phase, and to consider the coherent beam as a regular plane wave. In collinear case, both the coherent and incoherent beams propagate along the same axis  $z$  but angular spreading of the field components results in some spreading of the crossing angle  $\alpha$  between the wave vectors  $\mathbf{k}_{L1}$  and  $\mathbf{k}_{L2}$ . Obviously, this range of angles is from 0 to  $\theta_0$ . A similar situation is valid for crossed beams, where the crossing angle  $\alpha^*$  between the wave vectors  $\mathbf{k}_{L1}$  and  $\mathbf{k}_{L2}$  is determined as

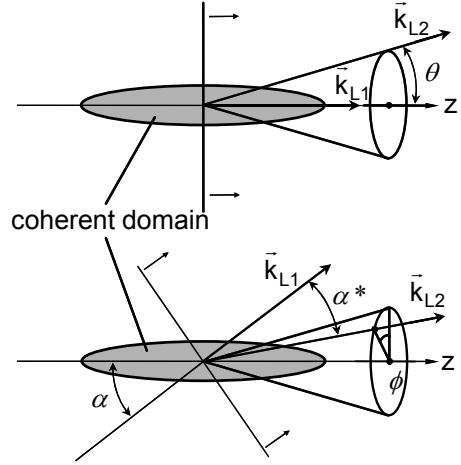


**Figure 22.** Wave-vector diagram for interaction of coherent and incoherent light fields: top, collinear excitation; bottom, noncollinear excitation.



$$\cos \alpha^* = \cos \theta \cos \alpha + \sin \theta \sin \alpha \cos \phi, \quad (19)$$

where  $\phi$  is the azimuth angle (see Fig. 22). For  $\alpha > \theta_0$ , the angle  $\alpha^*$  changes from  $\alpha - \theta_0$  to  $\alpha + \theta_0$ .

Simple geometrical consideration shown in Fig. 22 allows one to reduce the excitation problem for incoherent light field to the known problem of interaction of coherent waves propagated in an absorbing medium. Again, for a pair of crossed plain waves the concept of the cooperative line shift predicts the excitation profile as a Lorentzian peak shifted to the blue side of the resonance position (see previous section). The value of this shift is given by Eq. (18). For coherent beams the interaction geometry is characterized entirely by a given crossing angle  $\alpha$ , whereas for incoherent field an additional angular variable  $\theta$  enters the excitation problem.

Every partial configuration of interacting waves produces a Lorentzian excitation profile, but instead of a single Lorentzian peak for coherent waves a more broad excitation profile is expected for incoherent fields because of the angular spreading. In this sense, the excitation problem for interaction of coherent and incoherent waves is very similar to the three-photon excitation by coherent Bessel beams. For conical Bessel beams the three-photon excitation profile near the atomic resonance builds up as a superposition of multiple Lorentzians, where every individual Lorentzian corresponds to some spatial configuration of sub-beams from the fundamental light cone (see previous section). In the same manner, the excitation profile for interaction of coherent and incoherent waves builds up from multiple configurations of angled waves. This superposition includes all possible subscriptions of the wave vectors  $\mathbf{k}_{L2}$  within the cone of the angular spreading. Every elementary profile in this superposition has the same appearance of the atomic line, i.e., all profiles are Lorentzians with equal amplitudes and widths. This situation has been analyzed in detail in previous section and the same approach was used here.

Figure 23 shows the excitation profiles calculated for collinear and noncollinear interaction of coherent and incoherent beams. For the incoherent beam, a maximum spreading angle  $\theta_0 = 10^\circ$  was assumed. For collinear beams the angle  $\theta_0$  determines the red edge of the region (or the minimum value of available cooperative shift) where individual Lorentzians are located. This red edge is marked in Fig. 23. Note that the approach of equal Lorentzians is valid when  $\alpha > \theta_{\min}$ . Thus, the detuning  $\Delta_c$  in calculations was limited by the range  $\Delta_c < 200 \Gamma$ . For a larger detuning the ionization signal is reduced rapidly and the approach of equal Lorentzians breaks down since the medium becomes transparent for the sum-frequency light. In this case, a phase-matched VUV

emission near  $\lambda \approx 129$  nm exits the excitation region. This weak low-coherent VUV light is confined within a range of angles  $\theta < \theta_{\min}$ .

Superposition of multiple Lorentzians in collinear case produces an excitation profile peaked very close to the red edge of the region, where Lorentzians are spread. It agrees well with the experimental observations, where the excitation profile for collinear geometry demonstrated distinct evidence of noncollinearity with an effective crossing angle of  $9^\circ$ , which was very close to the experimental value  $\theta_0 \approx 10^\circ$ . The maximum of the calculated profile is located at  $\Delta_c \approx 125\Gamma$  that corresponds to about  $400 \text{ cm}^{-1}/\text{bar}$  for the  $6s'$  resonance. In terms of the dye laser wavelength, it gives the pressure-induced shift of  $4 \text{ nm}/\text{bar}$  and it is in good agreement with experimental findings. Qualitatively, formation of the peak near the red edge can be understood as follows.

First, for a uniform angular distribution of field components the spectral density of Lorentzian peaks is increased rapidly toward the resonance position. Second, due to axially symmetric excitation geometry, the Lorentzians for a given  $\theta$  enter superposition with an annular weighting factor  $\sin \theta$ . Thus, the envelope of superimposed Lorentzians gains intensity toward the region of large  $\theta$  and small detunings from the resonance.

Noncollinear excitation by two crossed coherent beams produces an excitation profile as a Lorentzian peak located on the blue side of the atomic resonance. This profile is shown in Fig. 23 for the crossing angle  $\alpha = 18^\circ$ , when the shift  $\Delta_c = 36\Gamma$ . For crossed coherent and incoherent beams, the crossing angle between the field components becomes spread within some range and a variable angle  $\alpha^*$  determines excitation geometry instead of a fixed angle  $\alpha$  (see Fig. 22). This crossing angle  $\alpha^*$  is given by Eq. (19), where  $\theta$  changes from 0 to  $\theta_0$  and  $\phi$  changes from  $0^\circ$  to  $360^\circ$ . The overall excitation profile is given by an integral of Lorentzian profiles over angles  $\theta$  and  $\phi$ . This excitation profile is shown in Fig. 23. Superposition of multiple

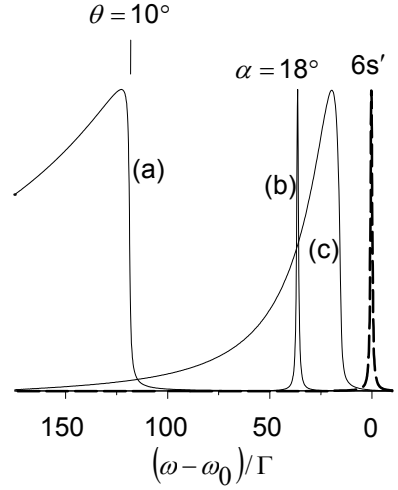


**Figure 23.** Numerical simulation of near-resonance excitation profiles: (a) collinear excitation by coherent and incoherent beams; (b) Lorentzian profile for two coherent beams with crossing angle  $\alpha = 18^\circ$ ; (c) coherent and incoherent beams with crossing angle  $\alpha = 18^\circ$ . The dashed line shows the resonance atomic line.

Lorentzians produces an excitation profile, which is peaked closer to the resonance than the Lorentzian profile for coherent beams. Again, it results from increased spectral density and weighting factors for elementary Lorentzians toward the region of maximum crossing angles  $\alpha^*$ , and thus minimum detunings from the resonance. The peak of the calculated profile is located at  $\Delta_c \approx 20 \Gamma$  that corresponds to a pressure-induced shift of  $64 \text{ cm}^{-1}/\text{bar}$  or  $0.64 \text{ nm}/\text{bar}$  in terms of the dye laser wavelength. This value is again in very good agreement with the shift of  $0.65 \text{ nm}/\text{bar}$  observed in experiment. Note distinct similarity of the ionization profile 3 in Fig. 23 and the ionization profiles for coherent Bessel beams (Fig. 13) calculated with the same approach of multiple elementary Lorentzian profiles distributed near the atomic resonance.

The angular spreading of field components in incoherent laser light is responsible for the red shift of ionization profiles with respect to the location of this peak in coherent beams. This difference is especially pronounced at small crossing angles, when the peak for collinear geometry has a large shift. For interaction of coherent and incoherent beams, the shift is smaller because of a significant local noncollinearity. In this case, the shift of the ionization peak in collinear case corresponds approximately to the maximum angle of spreading of the field components in the incoherent beam.

Sum-frequency field dominates the resonance excitation in an absorbing medium [82, 83, 115, 116, 118]. The evaluation of the excitation profiles was based on a simple geometrical consideration together with phase-matching requirements for the generated sum-frequency field, but did not include the length of coherent interaction. This gain length accounts for intensity of the ionization peaks but not for the shape of the excitation profiles. The length of coherent interaction, however, becomes a crucial factor for the on-resonance excitation, when the interference of the three- and the one-photon pathways determines resonance excitation. The evolution of the interfering sum-frequency field requires a certain (concentration dependent) propagation distance into the excitation zone. The drop in signal of the on-resonance excitation begins when the absorption length for the sum-frequency field becomes comparable with the length of coherent interaction [80, 118]. If this distance is too short for a complete evolution of the sum-frequency field in amplitude and phase, a complete cancellation is not established and laser photons drive the three-photon excitation of the atomic resonance. For incoherent light fields, the length of coherent interaction is determined by the mean size of coherent domains. Since domains are extended along the propagation axis, this length is reduced rapidly when crossing angle between coherent and incoherent beams is

increased (see Fig. 22). Considering the coherent domains as ellipsoids with axes  $d$  and  $\Delta z$ , the length  $L$  of interaction as a function of the crossing angle  $\alpha$  can be written as

$$L = \frac{d\Delta z}{\sqrt{\Delta z^2 \sin^2 \alpha + d^2 \cos^2 \alpha}}. \quad (20)$$

For  $\alpha = 90^\circ$  the length  $L = d$  is minimum and can be as short as a few wavelengths. For such extremely short gain length the contribution of sum-frequency field to the transition amplitude should be diminished significantly.

An incomplete cancellation of the atomic excitation is believed to be responsible for the observed deviations of the pressure-induced shift of the ionization peaks from a linear dependence (Fig. 21). In all experiments with angled beams, the shift becomes linear at an elevated gas pressure, but distinct deviations from this linear dependence occurred within a low-pressure region, where the peaks always had a smaller shift. An explanation of these observations is that the ionization signal at a low pressure contains a significant contribution from the uncanceled atomic resonance. At a low gas pressure, no cancellation occurs and a peak of the resonance excitation is registered. With an increased pressure, the sum-frequency field starts to develop. This field suppresses progressively the resonance excitation and increases the excitation on the blue wing of the atomic line. The resonance peak is very narrow (about 30 pm/bar in terms of the dye laser wavelength), therefore both on- and off-resonance components are registered together as a single peak with a small apparent shift. Further increase of pressure leads to a complete cancellation of the atomic resonance and the ionization profile becomes entirely due to the off-resonance sum-frequency field. Without contribution from the unshifted atomic peak, the dependence of pressure-induced shift becomes linear. Experiments have shown that a reduced apparent shift, and thus some contribution to the ionization profile from the uncanceled atomic peak, can be traced up to a pressure of about 100 mbar for the crossing angle  $\alpha = 18^\circ$ . With an increased  $\alpha$ , the length of the coherent interaction is reduced rapidly and achieves a minimum at  $\alpha = 90^\circ$ . Thus, with an appropriate spectral resolution, the use of crossed coherent and incoherent beams may give a reliable possibility to detect the atomic resonance lines free of interfering coherent effects.

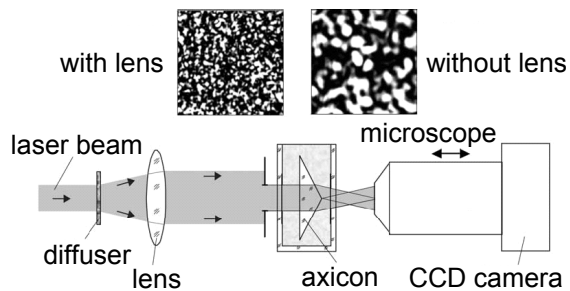
## 6. SPATIALLY INCOHERENT CONICAL LASER BEAMS

Important feature of conical beams is their extended excitation region. In coherent  $J_0$  Bessel beams, a nonlinear process is confined to the central lobe of the Bessel profile where light intensity is maximum. This high intensity focal line can be made much longer than the Rayleigh length of reference Gaussian beams. Spatial incoherence destroys regular Bessel or Gaussian patterns and the excitation volume in both cases is decomposed into multiple regions where some degree of coherence persists, but these coherent domains are mutually uncorrelated. The general beam geometry, however, is preserved and the focal region of conical beams remains extended along the beam axis. It means that the domain structure in incoherent conical beam differs significantly from that in the reference Gaussian beam. For any coherent nonlinear process the structure and characteristic dimensions of coherent domains in the focal region are of crucial importance. Therefore, a special study was carried out for a detailed characterization of the used coherent and incoherent beams.

### 6.1. Characterization of incoherent conical beams

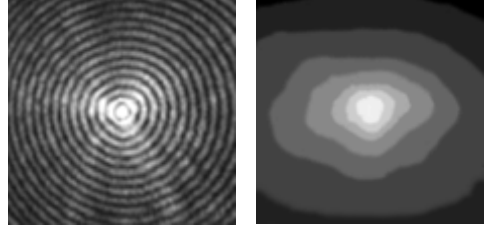
Characterization of partially coherent nondiffracting light beams was a subject of several theoretical studies (see, for example, [20, 46, 136 – 138] and references therein). In the present work, a simple empirical approach was used and all necessary parameters of the focal coherent domains were obtained from model experiments with laser beams of a variable spatial coherence. To have a basis for comparison, the same experimental procedure was applied also to the well-known Gaussian beams.

Figure 24 illustrates a schematic of experimental arrangement for the characterization of different laser beams. To match tightly



**Figure 24.** Schematic of experimental setup for characterization of laser beams. CCD pictures show the speckled patterns of scattered He–Ne laser beam on the entrance surface of the axicon with and without the collimating lens (each picture size is  $2 \times 2 \text{ mm}^2$ ).

focused conical beams with microscope optics, the inclination angle of beams was reduced with the aid of axicon immersion. The axicon with apex angle  $120^\circ$  was placed into an optical cuvette filled by distilled water. Such immersion reduced the inclination angle of conical beams to about  $4^\circ$ . The focal region of beams was imaged by a microscope and a CCD camera. Fig. 25 shows an



**Figure 25.** CCD pictures of the focal regions of conical beams: left, dye laser beam; right, XeCl laser beam. Each picture size is  $70 \times 70 \mu\text{m}^2$ .

example of intensity distributions in the focal region of the dye laser beam  $\lambda = 447 \text{ nm}$  and the UV beam  $\lambda = 308 \text{ nm}$  from XeCl laser. The last profile is shown in a scale of intensity reduced to 8 gradations. Spatially coherent beam of the dye laser produced the known pattern of a  $J_0$  Bessel beam, where the diameter of central maximum was  $4.81\lambda/2\pi \sin \alpha \approx 5 \mu\text{m}$ . Incoherent beam from the XeCl laser produced a smooth intensity distribution peaked on the beam axis. The width of profile was  $30 - 40 \mu\text{m}$  FWHM. The profile had very slow evolution along propagation direction and, to some extent, such incoherent conical beam can be considered as a particular case of propagation-invariant light fields.

The XeCl laser beam has poor temporal coherence and the time-integrated intensity profiles tell little about the structure of transient coherent domains in the focal region. Therefore, in model experiments examined was the pattern of stationary speckles formed with the aid of a He–Ne laser and a holographic diffuser. The diffuser with scattering angle  $30^\circ$  was illuminated by a He–Ne laser (see Fig. 24). A small part of scattered speckled beam was passed through a diaphragm and focused by axicon. The diffuser was placed at a distance of about 90 cm from the cuvette. In this case, the mean size  $d_0$  of speckles on the axicon was  $0.3 - 0.4 \text{ mm}$ . Additionally, a lens of focal length  $f = 27 \text{ cm}$  could be placed behind the diffuser as shown in Fig. 24. This lens collimated the scattered beam and reduced  $d_0$  by 3–4 times. The same elements were used in experiments with Gaussian beams, where a lens of focal length  $f = 35 \text{ mm}$  was placed instead of the cuvette with axicon. This lens gave the focusing angle  $\alpha = D/2f \approx 4^\circ$ , where  $D$  is the beam diameter. In all model experiments the condition  $\alpha \gg \theta$  was satisfied, where  $\theta$  is the divergence angle of speckled beams on focusing elements.

Fig. 26 shows the focal regions of beams in model experiments. Without the diffuser and collimating lens, the axicon focussing of coherent He-Ne beam produced the known pattern of a  $J_0$  Bessel beam with the central peak diameter of about  $7\text{ }\mu\text{m}$  (Fig. 26(a)). When the same beam was focused by the lens  $f = 35\text{ mm}$ , a Gaussian focal spot of about  $10\text{ }\mu\text{m}$  was formed (Fig. 26(b)). With the diffuser inserted, these Bessel and Gaussian profiles were decomposed into irregular patterns of multiple speckles (Fig. 26 (c) and (d)). Evolution of these patterns under propagation was examined by moving microscope along the beam axis.

The general structure of volume speckles in focused

incoherent Gaussian beams is well known. In the case here, the measured transverse size  $d$  and the length  $\Delta z_G$  of focal speckles were  $d = 5 - 10\text{ }\mu\text{m}$  and  $\Delta z_G = 0.2 - 0.3\text{ mm}$  in good agreement with simple estimates  $d \sim \lambda/\alpha$  and  $\Delta z_G \sim \lambda/\alpha^2$  [93]. Both  $d$  and  $\Delta z_G$  were insensitive to the transverse size  $d_0$  of input speckles since in all cases the condition  $\alpha \gg \theta$  was valid and the characteristic dimensions of focal speckles were determined entirely by the focusing angle  $\alpha$ . Fig. 26 shows that the focal speckles in incoherent conical beam have nearly the same transverse size  $d$  as in the reference Gaussian beam. It means that the same estimate  $d \sim \lambda/\alpha$  remains valid for conical beams. The length of speckles  $\Delta z$ , however, differed significantly from the Gaussian case. For large input speckles the length  $\Delta z = 5 - 8\text{ mm}$  was measured. This length was reduced to  $1.2 - 1.8\text{ mm}$  when input speckles were reduced by the collimating lens  $f = 27\text{ cm}$ . These results imply that  $\Delta z$  in conical beams is

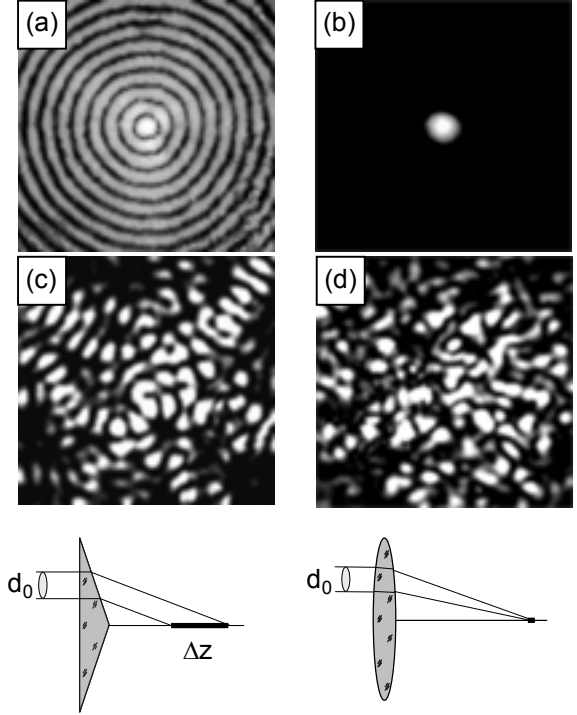


**Figure 26.** CCD pictures of the focal regions: (a) Bessel beam; (b) Gaussian beam; (c) spatially incoherent conical beam; (d) spatially incoherent Gaussian beam. Each picture size is  $70 \times 70\text{ }\mu\text{m}^2$ . Bottom: schematic of formation of coherent focal domains in conical and Gaussian beams.

proportional to the transverse size of input speckles or, more generally,  $\Delta z$  is proportional to the characteristic size of lateral wave-front correlations in the input beam. The focal speckles in conical beams are extended significantly along the beam axis so that  $\Delta z \gg d$  and  $\Delta z \gg d_0$ . It is fairly easy to see that such an extended  $\Delta z$  is formed as a projection of input correlation  $d_0$  toward the beam axis, when  $\Delta z \approx d_0 / \tan \alpha \approx d_0 / \alpha$  (see Fig. 26). It means that conical excitation geometry is able to produce very long correlated regions even for relatively small input correlations. Since  $d_0 \sim \lambda / \theta$  and  $\alpha \gg \theta$ , the ratio  $\Delta z / \Delta z_G \sim \alpha / \theta \gg 1$ . It indicates a significant advantage of conical beams in formation of very long coherent domains in the focal region as a key feature of these beams in the excitation of coherent nonlinear processes.

With the analytical guidance of model experiments, all necessary parameters of the dye and the XeCl laser conical beams are readily obtained. In the gas cell the coherent dye laser beam produces a  $J_0$  Bessel beam with the central peak diameter of about 2  $\mu\text{m}$  and 1  $\mu\text{m}$  for the beams  $\alpha = 10^\circ$  and  $\alpha = 17^\circ$ , respectively. The length  $L$  of this high intensity region is proportional to  $1/\tan \alpha$  and it was 10–12 mm for the beam  $\alpha = 10^\circ$  and 5–6 mm for the beam  $\alpha = 17^\circ$ . The incoherent UV beam from XeCl laser forms a conical beam, where the transient coherent domains have characteristic dimensions  $d \sim \lambda / \alpha$  and  $\Delta z \sim d_0 / \alpha$ . The corresponding values are  $d \approx 2 \mu\text{m}$ ,  $\Delta z \approx 2 \text{ mm}$  for  $\alpha = 10^\circ$ , and  $d \approx 1 \mu\text{m}$ ,  $\Delta z \approx 1 \text{ mm}$  for  $\alpha = 17^\circ$ . Note, that for small  $\alpha$  the lateral spatial correlations in the input beam produce very long longitudinal correlations in the focal region. In this case, the actual distance of coherent interaction becomes limited by the temporal coherence length of XeCl laser beam.

## 6.2. Experimental results with incoherent conical beams

General experimental procedure was the same as that used with spatially incoherent Gaussian beams. The ionization profiles in coherent–incoherent two-color excitation conical mode were compared with profiles measured in the same conditions under coherent one-color excitation and in ordinary excitation geometry of focused laser beams (see previous section). Fig. 27 demonstrates the arrangement of main optical elements for one- and two-color excitation by conical beams.

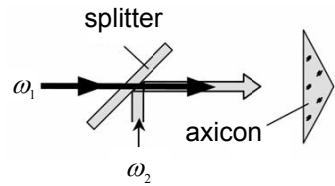


**Figure 27.** Schematic of two-color excitation geometry by conical beams.



In conical excitation geometry, the laser light is concentrated along an extended focal line instead of a much more compact excitation region of focused Gaussian beams. As a result, the local light intensity in conical beams is always much lower than in the reference Gaussian beams [139]. Simple estimates have shown that in the case here, the light intensity in conical beams was by at least an order of magnitude lower than in the focal region of beams considered in previous section. Therefore, no multiphoton atomic resonances of xenon like those shown in Fig. 3 and Fig. 18 were detected with conical beams even with maximum pulse energy available from the dye laser. However, with addition of the XeCl laser beam an intense ionization band appeared in spectra similar to the observations of previous section. With conical beams, quite a moderate laser pulse energy produced the same ionization signal as with beams focused by spherical optics. For example, the energy range in previous section was 1–1.2 mJ and 50–100  $\mu$ J for the dye and the excimer laser beams, respectively. For two-color conical beams, the same ionization signal was easily achieved with 1–1.2 mJ for the dye laser and 150–200  $\mu$ J for the excimer laser beam. Actually, the energy range for conical beams was even lower since minor uncontrolled misalignment of two long and thin focal lines reduced the overlap region and only a fraction of the total pulse energy contributed the ionization signal. For the reference one-color Bessel beam (QUI dye) the laser pulse energy was 0.3–0.4 mJ.

Figure 28 shows evolution of the ionization band with xenon pressure in conical beams  $\alpha = 10^\circ$ . Again, the ionization profiles have two distinct peaks, which correspond to two emission lines in XeCl laser spectrum (see Fig. 17). With conical beams, the dip in ionization profiles due to OH absorption in XeCl lasing spectrum could be traced up to a pressure of about 500 mbar, but no such feature was observed in experiments with Gaussian beams. It is again a consequence of relatively low light intensity in conical beams. The high light intensity in tightly focused Gaussian

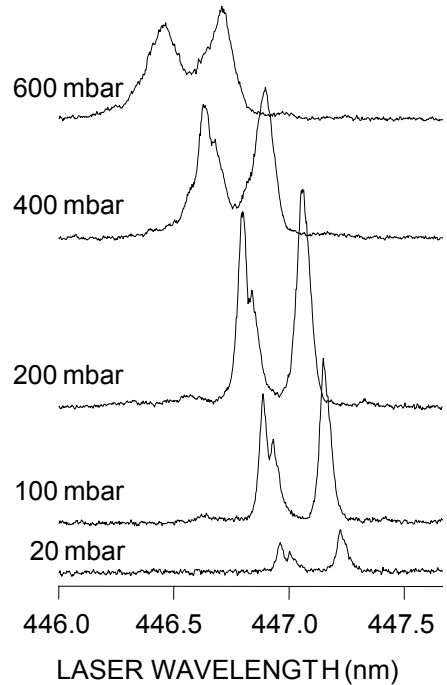


**Figure 28.** Wavelength scans of ionization signal in two-color conical beams  $\alpha = 10^\circ$ .

beams induced remarkable ac Stark broadening of the ionization peaks. In conical beams the light intensity was much lower. It diminished significantly the ac Stark broadening and allowed the observation of fine spectral features.

With an increased xenon pressure, the ionization peaks were broadened and shifted toward shorter wavelengths. The shift was linear with pressure and, in terms of the dye laser wavelength, the slope was 0.88 nm/bar for the beam  $\alpha = 10^\circ$  and 0.29 nm/bar for the beam  $\alpha = 17^\circ$ . Such a variation of pressure-induced shift with inclination angle is again a direct indication for a process where sum-frequency field is generated under noncollinear excitation and this field dominates the resonant excitation [117 – 119]. Fig. 29 demonstrates another example of ionization profiles for conical beams  $\alpha = 17^\circ$  in two- and one-color excitation modes. The profiles are shown in the scale of sum-frequency detuning from the  $6s'$  resonance position. For the two-color case this detuning was calculated with respect to the red peak of the ionization band. The one-color coherent excitation mode produced a  $J_0$  Bessel beam, where general features of near-resonance ionization profile are known [33, 113, 114] and have been considered above in section 4. This profile has a well-pronounced sharp peak followed by a tail toward shorter wavelengths. With an increased xenon pressure the peak is broadened and shifted off the resonance position. The same behavior demonstrate the two-color excitation profiles, but with smaller pressure-induced shift. The coherent one-color excitation gave the shift of  $30 \text{ cm}^{-1}/\text{bar}$  and  $95 \text{ cm}^{-1}/\text{bar}$  for the beams  $\alpha = 17^\circ$  and  $\alpha = 10^\circ$ , respectively. For two-color case the corresponding values were  $29 \text{ cm}^{-1}/\text{bar}$  and  $88 \text{ cm}^{-1}/\text{bar}$ .

Experiments with conical beams have shown the ability of conical excitation geometry to support effectively the sum-frequency generation in conditions of relatively low light intensity and a poor spatial coherence of one of the pumping fields. Low conversion efficiency is a common feature of incoherent beams in nonlinear frequency conversion processes. Moreover, the use of spatially incoherent laser beams may serve as a tool for

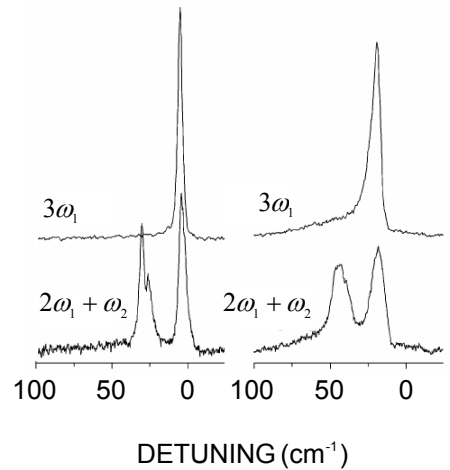


**Figure 29.** Sum-frequency  $3\omega$  and  $2\omega_1 + \omega_2$  excitation profiles for one- and two-color conical beams  $\alpha = 17^\circ$ . Left, xenon pressure 100 mbar; right, xenon pressure 600 mbar.

suppression the coherent transfer of energy from the pumping fields toward undesirable nonlinear processes (see previous section). However, there are distinct indications that the sum-frequency generation process is much less degraded in conical excitation geometry and, in agreement with previous observations [76], demonstrated conical beams here again their better tolerance in wave-front aberrations.

Wave-front irregularities in the input beams decompose the excitation volume into multiple mutually uncorrelated domains. The generated sum-frequency field gains intensity along the beam axis as long as an appreciable correlation of the pumping field components and phase matching between the fundamental and the generated sum-frequency fields are maintained. Decay of correlation destroys this coherent process and the evolution of sum-frequency field in amplitude is limited by the length of coherent focal domains. In tightly-focused incoherent Gaussian beams this gain length  $\Delta z_G$  can be made very short (a few microns) and it reduces significantly the overall efficiency of the wave-mixing process. Axicon focusing gives much lower light intensity within the focal line of a length  $L$ , but the correlation length  $\Delta z$  becomes extended significantly so that  $\Delta z \gg \Delta z_G$ . In two-color conical beams the ionization signal originates from the region, where the central lobe of the coherent Bessel beam  $\omega_1$  overlaps the transient coherent domains from the incoherent beam  $\omega_2$ . The ratio  $L/\Delta z$  (see above) indicates that only a few of such coherent domains are located within the central lobe of the Bessel beam at a given time moment. The four-wave process is driven within these embedded domains and the extended gain length  $\Delta z$  facilitates the build-up of sum-frequency field. For comparison, the focal volume of a Gaussian beam included in similar conditions up to  $10^3$  of small-scale transient domains. Obviously, it resulted in a much lower efficiency of the coherent four-wave process.

### 6.3. Analysis of experimental profiles

Analysis of excitation profiles for conical beams was carried out in the following manner. In two-color conical excitation geometry, the  $2\omega_1 + \omega_2$  process is driven by two superimposed light cones. Elementary configurations in this case involve two photons from one conical beam and one photon from another beam. Here again all possible combinations of fundamental photons contribute the excitation profile. Cylindrical symmetry of conical beams allows one to fix the azimuth angle  $\phi_3 = 0$  for the wave  $\omega_2$  and to consider further only the variations of  $\phi_1$  and  $\phi_2$  for two waves  $\omega_1$ .

When three crossed waves drive nonlinear polarization at  $\omega = 2\omega_1 + \omega_2$  within the negatively-dispersive side of an atomic state with resonance frequency  $\omega_0$ , the phase mismatch between the incident fields and the generated sum-frequency field vanishes at some detuning  $\Delta\omega = \delta_c = \omega - \omega_0$  from the resonance position. For a two-level system and far enough from the resonance position this detuning for any configuration of three crossed waves can be found from simple wave-vector diagrams. It gives

$$\Delta\omega = \frac{2\Delta_0(2+r)^2}{\sin^2 \alpha (1+2r - \cos(\phi_1 - \phi_2) - r \cos \phi_1 - r \cos \phi_2)}, \quad (21)$$

where  $r = \omega_2/\omega_1$ , and  $\Delta_0$  is given by Eq. (5). This general expression is valid also for some other excitation geometries. For example, for a one-color conical beam  $r = 1$  and Eq. (21) gives the known expression for the TH frequency shift in Bessel beams (Eq. 9).

Another example is the generation of sum-frequency field by two crossed beams [117 – 119]. In this case  $\phi_1 = \phi_2 = 180^\circ$  and Eq. (21) gives the detuning  $\Delta\omega$  as:

$$\Delta\omega = \frac{\Delta_0(2\omega_1 + \omega_2)^2}{2\omega_1\omega_2 \sin^2 \alpha} = \frac{\Delta_0(\lambda_1 + 2\lambda_2)}{\lambda_{mix}(1 - \cos 2\alpha)}, \quad (22)$$

where  $\lambda_{mix} = 2\pi c/(2\omega_1 + \omega_2)$ , and  $2\alpha$  is the crossing angle between two waves. Eq. (22) is the known expression for near-resonance two-color excitation profiles in crossed laser beams [117 – 119]. Owing to the noncollinear phase matching and circular symmetry of pumping fields, the sum-frequency emission forms an outgoing light cone with inclination angle  $\beta \leq \alpha$ . For a given spatial configuration of fundamental waves from the two light cones, the angle  $\beta$  is found from wave-vector diagram as

$$\tan \beta = \frac{\sqrt{2 + r^2 + 2\cos(\phi_1 - \phi_2) + 2r \cos \phi_1 + 2r \cos \phi_2}}{2 + r} \tan \alpha. \quad (23)$$

For  $r \leq 2$  the angle  $\beta$  changes from 0 to  $\alpha$ . For  $r = 1$  (one-color Bessel beam) the minimum value  $\beta = 0$  corresponds to a symmetrical configuration of three fundamental waves separated by the azimuth angle  $120^\circ$  from each other. This configuration gives also the minimum value of detuning  $\Delta\omega_{min} = 4\Delta_0/\sin^2 \alpha$ . For  $r = 2$  the same values of  $\Delta\omega_{min}$  and  $\beta = 0$

correspond to a planar configurations of the pumping waves, when  $\phi_1 = \phi_2 = 180^\circ$ . Further increase of  $r$  increases the gap between the resonance position and the nearest phase-matching point. For  $r > 2$  the angle  $\beta > 0$  for any configuration of fundamental photons.

All possible elementary configurations of the pumping fields contribute the overall near-resonance excitation and it makes very complex theoretical simulation of the excitation and ionization profiles. For one-color coherent conical beams the nonlinear response in the TH generation process can be derived from direct treatment of the scalar wave equation with the source field represented as a  $J_0$  Bessel beam [30, 31]. For some experimental conditions, when the absorption of generated TH is very strong, the ionization profile for a Bessel beam can be simulated as a superposition of equally-weighted Lorentzian profiles variously displaced in the negatively-dispersive side of atomic resonance (section 4). To some extent, the same approach can be applied also for two-color excitation by conical beams with large inclination angles  $\alpha$ , when the absorption of sum-frequency field is strong and the ionization peaks are located close to the atomic resonance. To carry out a more general analysis, another approach was used here [140]. In this approach, the spectral density of phase-matching points was considered for conical beams.

From (21) it follows, that any elementary configuration of pumping fields with given azimuth angles  $\phi_1$  and  $\phi_2$  can be characterized by a phase-matching point located at some detuning  $\delta_c$  from the atomic resonance. Since angles  $\phi_1$  and  $\phi_2$  have all possible choices from  $0^\circ$  to  $360^\circ$ , these phase-matching points are spread within a broad spectral region starting from some minimum detuning  $\Delta\omega_{\min}$  from the resonance. This spectral distribution can be characterized by spectral density function  $\rho(\omega)$  written in the following form:

$$\rho(\omega) = \int_0^{2\pi} \int_0^{2\pi} \delta[\omega - \Delta\omega(\phi_1, \phi_2) - \omega_0] d\phi_1 d\phi_2, \quad (24)$$

where  $\delta$  is the Dirac delta function, and  $\Delta\omega(\phi_1, \phi_2)$  is given by Eq. (21). Fig. 30 shows  $\rho(\omega)$  calculated as a function of dimensionless detuning  $(\omega - \omega_0)/\Gamma$  from the resonance. In numerical work, the cone angle was  $\alpha = 10^\circ$ . In addition to numerical calculations, the behavior of  $\rho(\omega)$  was also evaluated analytically near peculiar points. Calculation results demonstrate the general structure of near-resonance excitation profiles in different excitation conditions. The case  $r = 1$  corresponds to the known process of TH generation in Bessel beams. In good agreement with experimental observations the calculated TH profile has a distinct red edge and a sharp peak followed by a tail toward shorter

wavelengths. Note distinct similarity of  $\rho(\omega)$  at  $r = 1$  and the transverse phase-matching integral [30, 31] derived as the overlap of the TH Bessel beam and the cube of the fundamental Bessel beam. The maximum of  $\rho(\omega)$  occurs when  $\phi_1 = 180^\circ$  and  $\phi_2$  is arbitrary, or  $\phi_2 = 180^\circ$  and  $\phi_1$  is arbitrary, or  $|\phi_1 - \phi_2| = 180^\circ$ . According to (23) this maximum corresponds to  $\tan \beta / \tan \alpha = 1/3$  which is the known relation (4) between the cone angles  $\alpha$  and  $\beta$  for the maximum output of TH in Bessel beams [30, 31]. The maximum of  $\rho(\omega)$  is infinite similar to the maximum of the transverse phase-matching integral [30, 31]. In the case here, the divergence arises from the use of the  $\delta$ -function instead of an elementary excitation profile with a finite spectral width.

The red edge of the calculated profile for  $r = 1$  corresponds to the minimum value of detuning  $\Delta\omega_{\min}$ , when phase-matched TH can be generated by Bessel beams. In this case  $\beta = 0$  and the TH emission is directed along the beam axis. The spectral distance to the red edge  $\Delta\omega_{\min}$  is  $8/9$  of the distance to the maximum of excitation profile (see section 4). All other profiles with  $r \leq 2$  have the same position of the red edge.

In experiments the ratio  $r$  was 1.45. The calculation results show that the peak of the excitation profile is split into two maxima if  $r > 1$ . The blue maximum corresponds to a configurations of pumping field when  $|\phi_1 - \phi_2| = 180^\circ$ . A particular case here are planar configurations  $\phi_1 = 0$  and  $\phi_2 = 180^\circ$ , or  $\phi_1 = 180^\circ$  and  $\phi_2 = 0$  (recall that the field  $\omega_2$  is fixed at the azimuth angle  $\phi_3 = 0$ ). The blue maximum is shifted toward shorter wavelengths with an increased  $r$ . The red maximum has an opposite shift toward the red edge of the excitation profile. This maximum corresponds to the configurations of pumping fields when

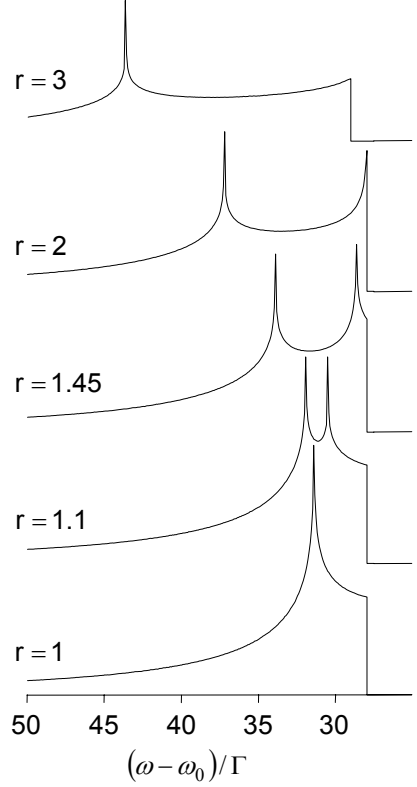


**Figure 30.** Spectral density  $\rho(\omega)$  of phase-matching points as a function of detuning from the resonance position for one- and two-color conical beams  $\alpha = 10^\circ$ .

$$\cos(\phi_1 - \phi_2) + r \cos \phi_1 + r \cos \phi_2 = 1 - 2r. \quad (25)$$

A particular case here is a planar configuration  $\phi_1 = \phi_2 = 180^\circ$ . For  $r = 1$  the red and the blue peaks coincide and (25) determines the relation between angles  $\phi_1$  and  $\phi_2$  for this single maximum of the excitation profile. The ratio of detunings  $\Delta\omega$  for the red and the blue maximum is  $(r+1)/2r$  and is thus independent of the inclination angle  $\alpha$  and the gas density. For our case of  $r = 1.45$  this ratio was 0.84. For given  $r$  and  $\alpha$ , the spectral distance between two peaks is proportional to  $\Delta_0/\sin^2 \alpha$  and is increased with gas pressure since  $\Delta_0$  is proportional to the gas number density  $N$ .

The calculation results have shown that two-color excitation by conical beams produces excitation profiles with two maxima in contrast to a single maximum for one-color Bessel beams. One of these two peaks is located closer to the resonance and has thus a smaller pressure-induced shift than the peak of the corresponding one-color Bessel beam. It agrees with experimental observations, where the ionization peak under two-color excitation had smaller shift than the peak of the reference Bessel beam. For example, for  $\alpha = 10^\circ$  the shift of 95 and 88  $\text{cm}^{-1}/\text{bar}$  was measured with one-color Bessel beam and two-color beams, respectively. Very similar results are obtained from calculation. Using the exact value of inclination angle  $\alpha = 10.3^\circ$ , the condition  $\phi_1 = \phi_2 = 180^\circ$ , and the value  $\Delta_0/N = 0.7 \text{ cm}^{-1}/\text{bar}$  for the  $6s'$  resonance of xenon, the shift of 99 and 90  $\text{cm}^{-1}/\text{bar}$  is obtained from Eq. (21) for the peak of one-color beam  $r = 1$  and the red maximum of two-color profile  $r = 1.45$ , respectively.

Calculation results predict the existence of a second peak located at a shorter wavelength. For the present case, when the pumping field  $\omega_2$  had two components, it means that the ionization profiles should actually contain two additional spectral components located at the blue side of main peaks. The spectral separation between each pair of peaks is relatively small and, from above consideration, the additional peaks could be detected at an elevated gas pressure with beams of small  $\alpha$ . Fig. 31 shows the excitation profiles measured under two-color excitation by beams  $\alpha = 10^\circ$  in dense xenon. Despite of relatively poor spectral resolution, distinct blue satellites can be recognized in spectra for each of two main peaks. The position of these satellites is in very good agreement with calculation results. In calculations, Eq. (21) was used together with condition  $|\phi_1 - \phi_2| = 180^\circ$  for the blue peak and  $\phi_1 = \phi_2 = 180^\circ$  for the red peak. The position of origins for main peaks was obtained from the extrapolation of experimental dependences to zero pressure.

Small magnitude of blue satellites can be understood from the following consideration. In experiments, the generated sum-frequency field was registered

through ionization of the target gas, but the efficiency of such method is reduced gradually when the excitation wavelength is tuned off the resonance position. Sum-frequency photons propagate, in general, at some angle with respect to the axis of pumping conical beams. It is easy to see from (21) and (23) that the inclination angle  $\beta$  for the phase matched sum-frequency field is increased together with an increased detuning  $\Delta\omega$  :

$$\tan \beta = \tan \alpha \sqrt{1 - \frac{4\Delta_0}{\Delta\omega \sin^2 \alpha}} . \quad (26)$$

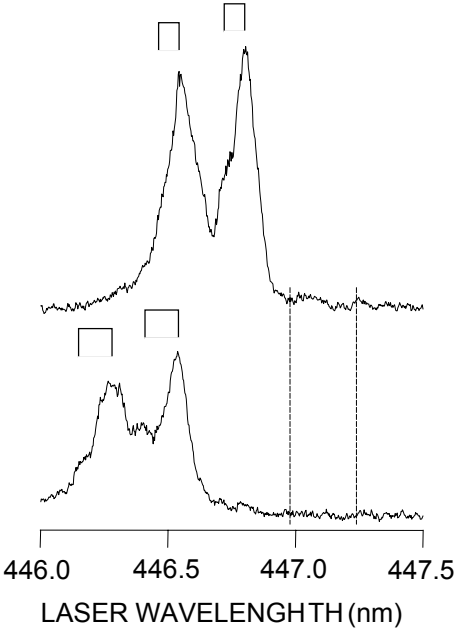


**Figure 31.** Wavelength scans of the ionization signal in two-color conical beams  $\alpha = 10^\circ$ . Upper trace – xenon pressure 500 mbar; lower trace – xenon pressure 800 mbar. Paired bars show the calculated positions of the two maxima of sum-frequency excitation profile. Vertical dashed lines indicate the position of origins for two main peaks.

Near the red edge of the excitation profiles the angle  $\beta$  is small and the generated sum-frequency photons propagate close to the axis of conical beams. These photons are absorbed entirely within the central lobe of the Bessel beam, where excited xenon atoms are effectively ionized by intense laser light. With an increased  $\Delta\omega$ , however, the absorption of sum-frequency photons gets weaker and the cone angle  $\beta$  is increased. As a result, a part of generated sum-frequency emission is absorbed outside the high-intensity core and the corresponding ionization signal is reduced. For the present case of  $r = 1.45$  the angle  $\beta$  is found from (23) as  $\tan \beta \approx 0.16 \tan \alpha$  for the red peak and  $\tan \beta \approx 0.42 \tan \alpha$  for the blue peak. Thus, for the red peak the ionization efficiency is higher and this peak dominates the ionization profile.



## 7. CONCLUSION

In the present work, the generation of sum-frequency field in a resonance-enhanced FWM process together with accompanying processes of multiphoton excitation and ionization of the target gas have been studied for different conical beams. A method of segmentation of the conical wave front has been introduced and demonstrated in selection of elementary sub-beam configurations from the conical light field. Two excitation modes were examined, where two-color mixed excitation by coherent and incoherent conical beams was compared with the case of a one-color coherent Bessel beam. Additionally, the results for the two-color combination of coherent and incoherent conical beams were compared with results obtained in ordinary geometry of beams focused by spherical optics.

In the simplest example, the generated wave-mixing field is the TH of a single-color excitation source. The generation of resonance-enhanced TH and multiphoton ionization in xenon under excitation by spatially coherent conical laser beams have been studied. Conical beams were produced by an axicon and the excitation geometry was controlled with the aid of different amplitude masks. Initial full-aperture conical beam formed the pattern of a diffraction-free Bessel beam. Masks selected partial configurations of the driving field from the fundamental light cone forming segmented or Mathieu amplitude profiles within the excitation region. It has been shown that for all conical beams an intense excitation band appears near the atomic resonance in REMPI spectra. This band is due to the generation of phase-matched resonance-enhanced TH. Significant transformations of this excitation band at segmentation of the input laser beam have been demonstrated.

Detailed analysis of the TH excitation profiles has been carried out. This analysis was based on a representation of the conical light beam as a superposition of multiple plain waves all inclined by a constant angle toward the propagation axis. In the TH generation process, the azimuthal angles of each of three interacting fundamental waves determine a partial component of the nonlinear polarization of the medium. The overall response of the medium builds up as a superposition of all such partial components. To analyze the TH excitation profiles, the concept of the cooperative line shift under noncollinear excitation has been used. In this concept, every partial configuration of the driving field produces in conditions of strong TH absorption a Lorentzian spectral profile (the so-called cooperative line) shifted from the atomic resonance. This Lorentzian is identical in width and height to the pressure-broadened atomic line but shifted from the resonance position by the

cooperative shift. For a full-aperture Bessel beam there is an infinite number of spatial configurations of interacting waves having different crossing angles and, thus, different values of the cooperative shift. The overall TH envelope for a Bessel beam builds up as a superposition of individual Lorentzians, where every Lorentzian corresponds to a given spatial configuration of pumping waves. This superposition of shifted lines has a formal similarity with inhomogeneous broadening of spectral response in a system where individual homogeneous components get spectral spreading and superposition of these components produces an inhomogeneous overall spectral profile. With this analogy, the whole TH ionization profile for a Bessel beam can be viewed as a result of “beam-geometry broadening” of the cooperative line.

Segmentation of the entrance beam reduces the number of available combinations of interacting waves. It results in specific transformations of the overall nonlinear response according to the phase-matching requirements for selected configuration of the pumping field. Again, the TH ionization profiles in segmented beams can be considered as a superposition of elementary Lorentzians with the appropriate values of the corresponding cooperative shift.

Numerical simulation of the TH excitation profiles for Bessel and segmented beams has been carried out and compared with experimental observations. This simulation was based on an approach of equally-weighted Lorentzians variously displaced by the cooperative shift. The overall spectral profile of harmonic generation was calculated as a superposition of these elementary Lorentzian profiles from all available spatial configurations of the pumping field. The calculation results have shown very good agreement with experimental data. The experimental and numerical results have shown that the use of conical excitation geometry together with apodization of the entrance beam allows one to realize different multibeam excitation schemes of a given spatial geometry and to vary the nonlinear response of the medium in a controlled manner.

The evolution of sum-frequency field in a four-wave mixing process requires certain coherence relations for the driving fields. If at least one of these fields has a low degree of spatial coherence, the coherent four-wave interaction is maintained within small-scale mutually uncorrelated domains. The length of coherent interaction within these domains depends on the coherent properties of the pumping field and excitation geometry. It gives a possibility of controlling the role and influence of the sum-frequency field in excitation processes.

Three-photon excitation of xenon atomic resonances by coherent and incoherent laser beams has shown distinct indications for the role of the sum-frequency field in the excitation processes. In a dense gas, this field is responsible for the appearance of intense ionization peaks on the blue wing of

atomic resonance. The shape and pressure-induced shift of these peaks follow the known pattern of the resonance-enhanced multiphoton excitation and ionization in crossed laser beams. However, with the use of an incoherent light several specific effects have been observed. For excitation by copropagating coherent beams no resonance ionization signal is expected. By contrast, intense ionization profiles were detected with incoherent light in any excitation geometry. The shift of the ionization peaks from the atomic resonance for an incoherent light always was smaller than the shift of the corresponding peak in a coherent excitation mode. These effects have been explained on the basis of a simple geometrical consideration, where the incoherent light field enters the excitation problem as a set of multiple plane waves variously displaced within some range of angles. This angular spreading of the field components supports a local noncollinearity of the four-wave interaction in any excitation geometry. Based on this approach, a numerical evaluation of near-resonance excitation profiles has been carried out and good agreement with experimental observation has been obtained.

Frequency conversion process may preserve a relatively high efficiency with incoherent beams if the nonlinear process is driven in conical excitation geometry instead of ordinary geometry of focused beams. Experiments have shown that two-color excitation by conical beams provides an effective FWM process even in conditions of a poor spatial coherence of one of the pumping fields. Moreover, the output of sum-frequency field (registered through ionization of the target gas) achieved easily the same level as in reference Gaussian beams despite of a much lower light intensity in conical beams. Simple model experiments have shown that such an increase of internal efficiency is due to a much extended gain length in incoherent conical beams. This extended length results from conical excitation geometry, where the coherent focal domains are formed as projections of input lateral correlations toward the beam axis. In a two-color excitation mode, the FWM process is driven within the central lobe of the fundamental Bessel beam. It provides the spatial selection of a few of long coherent domains from the incoherent field. In some sense, such conical excitation geometry allows one to preserve a relatively high degree of coherence for excitation processes even with input beams containing multiple wave-front aberrations. For comparison, in tightly focused spatially incoherent Gaussian beams the gain length is much smaller and the two-color excitation volume consists of a very large number of small uncorrelated domains from the incoherent beam. It reduces significantly the efficiency of coherent processes.

Numerical simulation has shown that excitation by two-color conical beams results in a specific doublet structure of sum-frequency excitation profiles. The

spectral separation between the two maxima of these profiles depends on the inclination angle of conical beams, the gas density and the ratio of frequencies for the pumping fields. For a one-color Bessel beam both maxima coincide and give a single peak of the resonance-enhanced TH. The results of numerical simulations for one- and two-color conical beams have shown very good agreement with experimental observations.

## SUMMARY

Resonance-enhanced generation of sum-frequency field in a four-wave mixing process and multiphoton ionization of xenon under excitation by different conical laser beams (full-aperture Bessel and segmented beams) have been studied. Two excitation modes have been employed where use was made of either spatially coherent beams or superimposed coherent and incoherent beams. A method of segmentation of the conical wave front has been introduced and demonstrated in selection of elementary sub-beam configurations from the conical light field. It has been shown that under one-color excitation by coherent conical beams, any segmentation of the conical wave front results in specific transformations of the third-harmonic excitation profiles. The concept of cooperative line shift under noncollinear excitation has been used to analyze these transformations. It has been shown that in conical light beams the third-harmonic excitation profiles can be viewed as a superposition of multiple homogeneous Lorentzians variously displaced by the cooperative shift. Each of these Lorentzians is identical to pressure-broadened atomic line but shifted from the resonance position by an applicable value of the cooperative shift. In segmented beams, it is possible to select different homogeneous spectral components from the overall excitation profile.

Two-color excitation by spatially coherent and incoherent conical laser beams has been compared with the two-color excitation in an ordinary geometry of focused beams and in one-color Bessel beams. It has been shown that with incoherent laser beams the four-wave mixing process is much less degraded in conical excitation geometry where a relatively efficient generation of sum-frequency field can be obtained despite of multiple wave-front aberrations. Such a tolerance of conical beams results from their specific structure of coherent focal domains, which are extended significantly along the beam axis and it preserves a relatively high degree of coherence for excitation of nonlinear processes. Numerical simulation of sum-frequency excitation profiles for one- and two-color conical beams has been carried out and good agreement with experimental observations has been obtained.

## SUMMARY IN ESTONIAN

### **Liitsageduse genereerimine ning paljufootoniline ionisatsioon ksenoonis kooniliste laserkiirekimpudega ergastamisel**

Käesolevas töös on uuritud resonantselt võimendatud liitsageduse genereerimist nelja optilise laine mittelineaarse segunemisel ning paljufootonilist ionisatsiooni ergastades ksenooni erinevate kooniliste laserkiirekimpudega (täisapertuursed Besseli ning segmenteeritud kiirekimpud). On kasutatud ning võrreldud kahte ergastusmoodust: ruumiliselt koherentsete laserkiirekimpudega ning kahevärvilise koherentse ja mittekoherentse kiirekimpude superpositsiooniga. On välja pakutud meetod koonilise valguslaine segmenteerimiseks, mille abil demonstreeriti elementaarsete valguslaine konfiguratsioonide selekteerimist koonilistest lainefrondist. On näidatud, et koonilise lainefrondi segmenteerimine viib spetsiifilistele kolmanda harmoonilise ergastusspektrite transformeeru-544mistele. Neid transformeerumisi on analüüsitud kasutades joone kooperatiivse nihke kontseptsiooni mittekollineaarsel ergastamisel. On näidatud, et koonilistes valguskiirekimpudes võib kolmanda harmoonilise ergastusspektrit vaadelda paljude elementaarsete Lorentzi profiiliga joonte superpositsioonina. Iga nendest lorentziaanidest on kooperatiivne joon, mis on identne rõhuga laienenud aatomjoonele, kuid resonantsist nihutatud kooperatiivse nihke võrra. Segmenteeritud laserikiirekimpude abil on võimalik välja selekteerida erinevad elementaarsed komponendid kolmanda harmoonilise ergastusspektrist.

Kahevärvilist ergastust koherentse ning mittekoherentse koonilise laserkiirekimpude superpositsiooniga on võrreldud samasuguse ergastusega tavalise fokuseerimise tingimustes ning ühevärvilises koherentses Besseli kiires. On näidatud, et koonilise ergastusgeomeetria korral on nelja laine mittelineaarne segunemine suhteliselt tolerantne lainefrondi aberratsioonide suhtes ning see tagab üsna efektiivse liitsageduse genereerimise tingimustes, kus tavalised fokuseeritud laserikiirekimbud on ebaefektiivsed. Selline kooniliste kiirekimpude omadus põhineb spetsiifilisel koherentsete domeenide struktuuril fokaalruumalas, kus need domeenid on tunduvalt välja venitatud kooniliste kiirekimpude telje suunas. See võimaldab säilitada suhteliselt suurt koherentsuse pikkust ning tagab mittelineaarsete protsesside efektiivsuse isegi tunduvalt moonutatud laserivalguse lainefrondi korral. Liitsageduse ergastusprofiilide teoreetiline modelleerimine andis väga hea kooskõla eksperimendi tulemustega.

## REFERENCES

1. Durnin J., *J. Opt. Soc. Am.*, **A4**, 651, 1987.
2. Durnin J., Micely J., Eberly Jr. and J., *Phys. Rev. Lett.*, **58**, 1499, 1987.
3. Durnin J., Micely J., Eberly Jr. and J., *Opt. Lett.*, **13**, 79, 1988.
4. Herman R. M. and Wiggins T. A., *J. Opt. Soc. Am.*, **A8**, 932, 1990.
5. Jabczynski J. K., *Opt. Comm.*, **77**, 292, 1990.
6. Cox A. J. and Dibble D. C., *Appl. Opt.*, **30**, 1330, 1991.
7. MacDonald R. P., Chrostowski J., Boothroyd S. A., and Syrett B. A., *Appl. Opt.*, **32**, 6470, 1993.
8. Rosen J., Salik B., and Yariv, A., *J. Opt. Soc. Am.*, **A12**, 2446, 1995.
9. Vasara, A., Turunen, J., and Friberg, A. T., *J. Opt. Soc. Am.*, **A6**, 1748, 1989.
10. Lee H. S., Stewart B. W., Will D., and Fenichel H., *Appl. Phys. Lett.* **59**, 3096, 1991.
11. Cox A. J. and Dibble D. C., *J. Opt. Soc. Am.*, **A9**, 282, 1992.
12. Horva'th Z. L., Erde'lyi M., Szabo' G., Bor Z., Kittel F. K., and Cavallaro J. R., *J. Opt. Soc. Am.*, **A14**, 3009, 1997.
13. Niggel, L., Lanzl T., and Maier, M., *J. Opt. Soc. Am.*, **A14**, 27, 1997.
14. Vahimaa P., Kettunen V., Kuittinen M., Turunen J., and Friberg A. T., *J. Opt. Soc. Am.*, **A14**, 1817, 1997.
15. Davis J. A., Carcole E., and Cottrell D. M., *Appl. Opt.*, **35**, 593, 1996.
16. Zeldovich, Ya. B., Mulchenko, B. F., and Pilipetskii, N. F., *Zh. Eksp. Teor. Fiz.*, **58**, 793, 1970 [*Sov. Phys. JETP*, **31**, 425, 1970].
17. Tremblay, R., D'astous, Y., Roy, G., and Blanchard, M., *Opt. Commun.*, **28**, 193 1979.
18. Korobkin, V. V., Marin, M. Yu., Pil'skii, V. I., Polonskii, L. Ya., and Pyatnitskii, L. N., *Sov. J. Quantum Electron*, **15**, 631, 1985.
19. Andreev, N. E., Aristov, Yu. A., Polonsky, L. Ya., and Pyatnitsky, L. N., *Zh. Eksp. Teor. Fiz.*, **100**, 1756, 1991 [*Sov. Phys. JETP*, **73**, 969, 1991].
20. Gori, F., Guattari, G., and Padovani, C., *Opt. Commun.*, **64**, 491, 1987.
21. Herman R. M. and Wiggins T. A., *Appl. Opt.*, **37**, 3398, 1998.
22. Bagini, V., Frezza, F., Santarsiero, M., Schettini, G., and Schirripa Spagnolo, G., *J. of Modern Optics*, **43**, 1155, 1996.
23. Ojeda-Castañeda, J., Escalera, J. C., and Yzuel, M. J., *Opt. Commun.*, **114**, 189, 1995.
24. Palma C., Cincotti G., Guattari G., and Santarsiero M., *J. Modern Optics*, **43**, 2269, 1996.
25. Jiang Z.-P., *Opt. Commun.*, **125**, 207, 1996.
26. Mishra S. R., *Opt. Commun.*, **85**, 159, 1991.
27. Borghi R. and Santarsiero M., *Opt. Lett.*, **22**, 262, 1997.
28. Borghi R., Santarsiero M., and Gori F., *J. Opt. Soc. Am.*, **A14**, 23, 1997.
29. Glushko, B., Kryzhanovsky, B., and Sarkisyan, D., *Phys. Rev. Lett.*, **71**, 243, 1993.
30. Tewari, Surya P., Huang, H., and Boyd, R. W., *Phys. Rev.*, **A51**, R2707, 1995.
31. Tewari, Surya P., Huang, H., and Boyd, R. W., *Phys. Rev.*, **A54**, 2314, 1996.
32. Peatross, J., Chaloupka, J. L., and Meyerhofer, D. D., *Opt. Lett.*, **19**, 942, 1994.
33. Peet, V. E. and Tsubin, R. V., *Phys. Rev.*, **A56**, 1613, 1997.
34. Paterson, C. and Smith, R., *Opt. Commun.*, **124**, 121, 1996.

35. Lee, H. S., Stewart, B. W., Choi, K., and Fenichel, H., *Phys. Rev.*, **A49**, 4922, 1994.
36. Arlt J. and Dholakia K., *Opt. Commun.*, **177**, 297, 2000.
37. Jarutis V., Paškauskas R., and Stabinis A., *Opt. Commun.*, **184**, 105, 2000.
38. Peet, V. E., Garrett, W. R., and Shchemeljov, S. V., *Phys. Rev.*, **A63**, 023804 2001.
39. Gutiérrez-Vega, J. C., Iturbe-Castillo, M. D., and Cávez-Cerda, S., *Opt. Lett.*, **25**, 1493 2000.
40. Gutiérrez-Vega, J. C., Iturbe-Castillo, M. D., Ramírez, G. A., Tepichin, E., Rodríguez-Dagnino, R. M., and Cávez-Cerda, S., *Opt. and Phot.*, **37**, 2000.
41. Gutiérrez-Vega, J. C., Iturbe-Castillo, M. D., Ramírez, G. A., Tepichin, E., Rodríguez-Dagnino, R. M., and Cávez-Cerda, S., *Opt. Commun.*, **195**, 35 2001.
42. Dartora, C. A., Zamboni-Rached, M., Norbrega, K. Z., Recami, E., and Hernández-Figueroa, H. E., *Opt. Commun.*, **222**, 75, 2003.
43. Butkus, R., Gadonas, R., Janušonis, J., Piskarskas, A., Regelskis, K., Smilgevičius, V., and Stabinis, A., *Opt. Commun.*, **206**, 201, 2002.
44. Vicari, L., *Opt. Commun.*, **70**, 263, 1989.
45. Ruschin S., *J. Opt. Soc. Am.*, **A11**, 3224, 1994.
46. Turunen, J., Vasara, A., and Friberg, A. T., *J. Opt. Soc. Am.*, **A8**, 282, 1991.
47. Ostrovsky, A. S., Martinez-Niconoff, G., and Ramirez-San-Juan, J. C., *Opt. Commun.*, **207**, 131, 2002.
48. Ostrovsky, A. S., Martinez-Niconoff, G., and Ramirez-San-Juan, J. C., *J. Opt. A: Pure Appl. Opt.*, **5**, S276, 2003.
49. Franken, P. A., Hill, A. E., Peters, C. W., and Weinreich, G., *Phys. Rev. Lett.* **7**, 118, 1961.
50. Wulle, T. and Herminghaus, S., *Phys. Rev. Lett.*, **70**, 1401, 1993.
51. Jarutis, V., Matijošius, A., Smilgevičius, V., and Stabinis, A., *Opt. Commun.*, **185**, 159, 2000.
52. Velchev, I. and Ubachs, W., *Opt. Lett.*, **26**, 530, 2001.
53. Altucci, C., Bruzzese, R., D'Antuoni, D., De Lisio, C., and Solimeno, S., *J. Opt. Soc. Am.*, **B17**, 34, 2000.
54. Altucci, C., Bruzzese, R., De Lisio, C., Porzio, A., Solimeno, S., and Tosa, V., *Opt. And Lasers in Engineering*, **37**, 565, 2002.
55. Sogomonian, S., Barille, and R., Rivoire, G., *Opt. Commun.*, **157**, 182, 1998.
56. Vaičaitis, V., Stabinis, A., Marcinkevičius, A., and Jarutis, V., *Opt. Commun.*, **178**, 461, 2000.
57. Biswas, D. J., Nilaya, J. P., and Danailov, M. B., *Opt. Commun.*, **226**, 387, 2003.
58. Klewitz, S., Sogomonian, S., Woerner, M., and Herminghaus, S., *Opt. Commun.*, **154**, 186, 1998.
59. Gadonas, R., Jarutis, V., Marcikevičius, A., Smilgevičius, V., and Stabinis, A., *Opt. Commun.*, **167**, 299, 1999.
60. Gadonas, R., Jarutis, V., Marcikevičius, A., Smilgevičius, V., Stabinis, A., and Vaičaitis, V., *Opt. Commun.*, **169**, 189, 1999.
61. Shinozaki, K., Xu, Ch., Sasaki, H., and Kamijoh, T., *Opt. Commun.*, **133**, 300, 1997.
62. King, T. A., Hogervorst, W., Kazak, N. S., Tugbaev, V. A., Belyi V. N., Khilo N. A., and Ryzhevich, A. A., *Non. Phen. in Complex Systems.*, **2**, 54, 1999.



63. King, T. A., Hogervorst, W., Kazak, N. S., Khilo N. A., and Ryzhevich, A. A., *Opt. Commun.*, **187**, 407, 2001.
64. Piskarskas, A., Smilgevičius, V., Stabinis, A., and Jarutis, V., *Opt. Lett.*, **24**, 1053, 1999.
65. Piskarskas, A., Stabinis, A., Vaičaitis, V., and Jarutis, V., *Opt. Commun.*, **158**, 298, 1998.
66. Pyragaite, V., Regelskis, K., Smilgevičius, V., and Stabinis, A., *Opt. Commun.*, **257**, 139, 2006.
67. Belyi V. N., Kasak, N. S., and Khilo N. A., *Quantum Electron.*, **30**, 753, 2000.
68. Caron, C. F. R. and Potvliege, R. M., *J. Opt. Soc. Am.*, **B16**, 1377, 1999.
69. Niggel, L. and Maier, M., *Opt. Commun.*, **154**, 65, 1998.
70. Golub, I., *Opt. Lett.*, **15**, 305, 1990.
71. Golub, I., *Opt. Lett.*, **20**, 1847, 1995.
72. Klewitz, S., Leiderer, P., Herminghaus, S., and Sogomonian, S., *Opt. Lett.*, **21**, 248, 1996.
73. Manz, T., Schwarz, U. T., and Maier, M., *Opt. Commun.*, **235**, 201, 2004.
74. Niggel, L. and Maier, M., *Opt. Lett.*, **22**, 910, 1997.
75. Sogomonian, S., Klewitz, S., and Herminghaus, S., *Opt. Commun.*, **139**, 313, 1997.
76. Piskarskas, A., Smilgevičius, V., and Stabinis, A., *Opt. Commun.*, **143**, 72, 1997.
77. Miller, J. C. and Compton, R. N., *Phys. Rev.*, **A25**, 2056, 1982.
78. Miller, J. C., Compton, R. N., Payne, M. G., and Garrett, W. R., *Phys. Rev. Lett.*, **45**, 114, 1980.
79. Glowina, J. H., and Sander, R. K., *Phys. Rev. Lett.*, **49**, 21, 1982.
80. Payne, M. G. and Garrett, W. R., *Phys. Rev.*, **A26**, 356, 1982.
81. Payne, M. G., Garrett, W. R., and Ferrell, W. R., *Phys. Rev.*, **A34**, 1143, 1986.
82. Payne, M. G. and Garrett, W. R., *Phys. Rev.*, **A28**, 3409, 1983.
83. Jackson, D. J., Wynne, J. J., and Kes, P. H., *Phys. Rev.*, **A28**, 781, 1983.
84. Charalambidis, D., Stockdale, J. A. D., and Fotakis, C., *Z. Phys.*, **D32**, 191, 1994.
85. Charalambidis, D., Xing, X., Petrakis, J., and Fotakis, C., *Phys. Rev.*, **A44**, R24, 1991.
86. Xing, X., Charalambidis, D., Koutsourelaki, E., and Fotakis, C., *Phys. Rev.*, **A47**, 2296, 1993.
87. Garrett, W. R., Henderson, S. D., and Payne, M. G., *Phys. Rev.*, **A35**, 5032, 1987.
88. Damany N., Laporte P., J.-L. Subtil, and H. Damany, *Phys. Rev. A* **32**, 3418, 1985.
89. Peet V. E., *Phys. Rev. A* **51**, 3982, 1995.
90. Payne, M. G., Miller, J. C., Hart, R. C., and Garrett, W. R., *Phys. Rev.*, **A44**, 7684, 1991.
91. Reintjes, J. F., *Nonlinear Optical Parametric Processes in Liquids and Glasses*, Academic Press, New York, 1984.
92. Shen, Y. R., *Principles of Nonlinear Optics*, John Wiley & Sons, 1984.
93. Boyd R. W., *Nonlinear Optics*, Academic Press, 2002.
94. Born M. and Wolf E., *Principles of Optics*, 7<sup>th</sup> edition, Cambridge Univ. Press, 2002.
95. Hanna D. C., Yuratich M. A., and Cotter D., *Nonlinear Optics of Free Atoms and Molecules*, Springer-Verlag, 1979.
96. Caron, C. F. R. and Potvliege, R. M., *J. Opt. Soc. Am.*, **B15**, 1096, 1998.

97. Payne, M. G., Ferrell, W. R., and Garrett, W. R., *Phys. Rev.*, **A27**, 3053, 1983.
98. Ferrell, W. R., Payne, M. G., and Garrett, W. R., *Phys. Rev.*, **A35**, 5020, 1987.
99. Jackson, D. J. and Wynne, J. J., *Phys. Rev. Lett.*, **49**, 543, 1982.
100. Compton, R. N. and Miller, J. C., *J. Opt. Soc. Am.*, **B2**, 355, 1985.
101. Blazewicz, P. R. and Miller, J. C., *Phys. Rev.*, **A38**, 2863, 1988.
102. Peet, V. and Shchemel'ov, S., *Phys. Rev.*, **A68**, 043411, 2003.
103. Aron K. and Johnson P. M., *J. Chem. Phys.* **67**, 5099, 1977.
104. Blazewicz, P. R., M. G. Payne, W. R. Garrett, and Miller, J. C., *Phys. Rev.*, **A34**, 5171, 1986.
105. Payne, M. G., Garrett, W. R., and Baker H. C., *Chem. Phys. Lett.*, **75**, 468, 1980.
106. Elk M., Lambropoulos P., and Tang X., *Phys. Rev.*, **A44**, R31, 1991.
107. Tewari S.P. and Agarwal C.S., *Phys. Rev. Lett.* **56**, 1811, 1986.
108. Hilbig, R. and Wallenstein, R., *IEEE J. Quantum Electron.*, QE-17, 1566, 1981.
109. Vallee, F., de Rougemont, F., and Lukasil, J., *IEEE J. Quantum Electron.*, QE-19, 1331, 1983.
110. Kutzner, J. and Zacharias, H., *Appl. Phys.*, **B66**, 571, 1998.
111. Kung A. H., *Appl. Phys. Lett.* **25**, 653, 1974.
112. Mahon R., McIlrath T. J., Myerscough V. P., and Koopman D. W., *IEEE J. Quantum Electron.* **QE-11**, 287, 1975.
113. Peet, V. E., *Phys. Rev.*, **A53**, 3679, 1996.
114. Garrett, W. R. and Peet, V. E., *Phys. Rev.*, **A61**, 063804, 2000.
115. Friedberg, R., Hartmann, S. R., and Manassah, J. T., *J. Phys. B: At. Mol. Opt. Phys.*, **22**, 2211, 1989.
116. Friedberg, R., Hartmann, S.R., and Manassah, J.T., *Phys. Rev.*, **A39**, 93, 1989.
117. Garrett, W. R., Hart, R. C., Wray, J. E., Datskou, I., and Payne, M. G., *Phys. Rev. Lett.*, **64**, 1717, 1990.
118. Payne, M. G. and Garrett, W. R., *Phys. Rev.*, **A42**, 1434, 1990.
119. Payne, M. G., Garrett, W. R., Hart, R. C., and Datskou, I., *Phys. Rev.*, **A42**, 2756, 1990.
120. Garrett, W. R., Hart, R. C., Wray, J. E., Datskou, I., and Payne, M. G., *Phys. Rev.*, **A42**, 1434, 1990.
121. Ferrell, W. R., Payne, M. G., and Garrett, W. R., *Phys. Rev.*, **A36**, 81, 1987.
122. Peet, V. E. and Shchemel'ov, S. V., *Phys. Rev.*, **A67**, 013801, 2003.
123. Murty, M.V., *J. Opt. Soc. Am.*, **54**, 1187, 1964.
124. Mandel, L. and Wolf, E., *Optical Coherence and Quantum Optics*, 1st ed. (Cambridge University, Cambridge, UK), 1995.
125. McCutchen, C. W., *J. Opt. Soc. Am.*, **56**, 727, 1966.
126. Biegen, J.E., *Opt. Lett.*, **19**, 1690, 1994.
127. Rosen, J. and Yariv, A., *Opt. Commun.*, **117**, 8, 1995.
128. Rosen, J. and Yariv, A., *J. Opt. Soc. Am.*, **A13**, 2091, 1996.
129. Rosen, J. and Takeda, M., *Appl. Opt.*, **39**, 4107, 2000.
130. Tellinghuisen, J., Hoffmann, J. M., Tisone, G. C., and Hays, A. K., *J. Chem. Phys.*, **64**, 2484, 1976.
131. Sur, A., Hui, A. K., and Tellinghuisen, J., *J. Mol. Spectrosc.*, **74**, 465, 1979.
132. Berik, E.B., Vill, A.A., Davidenko, V.A., Mikhelsoo, V.T., and Tsarenko, S.A., in *Proceedings of International Conference Lasers-82, New Orleans, USA*, edited by R.C. Powell (STS Press, McLean, 1983), p. 365.
133. Garrett, W. R., Henderson, S. D., and Payne, M. G., *Phys. Rev.*, **A34**, 3463, 1986.

134. Kruit, P., Kimman, J., Muller, H. G., and Van der Wiel, M. J., *J. Phys.*, **B16**, 937, 1983.
135. Berman, P.R. and Lamb, W.E., *Phys. Rev.*, **187**, 221, 1969.
136. Borghi, R., *IEEE J. Quantum. Electron.*, **35**, 849, 1999.
137. Kim, Hyuntae, Kim, Hyoung-Joo, Kim, Kisik, and Park, Dae-Yoon, *J. Korean Phys. Soc.*, **37**, 713, 2000.
138. Ostrovsky, A. S., Martinez-Niconoff, G., and Ramirez-San-Juan, J. C., *Opt. Commun.*, **195**, 27, 2001.
139. Korobkin, V. V., Polonskii, L. Ya., Poponin, V. P., and Pyatniskii, L. N., *Kvantovaya Elektron. (Moscow)*, *Sov. J. Quantum Electron.*, **16**, 178, 1986.
140. Peet, V. and Shchemel'ov, S., *Opt. Commun.*, **246**, 451, 2005.

## **ACKNOWLEDGEMENTS**

I have a great pleasure to thank people, which contributed to the completion of this thesis.

I wish to thank my supervisor Dr. Victor Peet for initiating all these investigations, continuous support, help and advice.

I also wish to thank all the people from the Laboratory of Laser Techniques of Institute of Physics of Tartu University, whose support and advice helped me a lot.

## **PUBLICATIONS**

V. Peet, W. R. Garrett and S. Shchemel'gov,  
Near-resonance three-photon excitation profiles  
in xenon with segmented conical beams, *Phys. Rev.*,  
**A63**, 023804 (5 pp), 2001.

V. Peet and S. Shchemel'gov, Spectral and spatial characteristics  
of third-harmonic generation in conical light beams, *Phys. Rev.*,  
**A67**, 013801 (7 pp), 2003.

V. Peet and S. Shchemel'gov, Three-photon resonant atomic excitation  
in spatially incoherent laser beams, *Phys. Rev.*,  
**A68**, 043411 (8 pp), 2003.

V. Peet and S. Shchemel'gov, Sum-frequency generation and multiphoton ionization  
in spatially incoherent conical laser beams, *Opt. Commun.*,  
**246**, pp 451–463, 2005.

# **CURRICULUM VITAE**

## **Sergey Shchemelyov**

Birth date and place: 14.12.1977, Narva, Estonia  
Address: Institute of Physics, University of Tartu, Riia 142, 51014  
Tartu, Estonia  
Phone: +372 56675736  
E-mail: sergeys@ldi.ee

## **Education**

2000–2002: M.Sc. (optics and spectroscopy), University of Tartu  
1996–2000: B.Sc. (experimental physics), University of Tartu  
1993–1996: School of Exact Sciences of Tartu University  
1985–1996: Narva Kesklinna High School

## **Work Experience**

2006– Laser Diagnostic Instruments Ltd, researcher  
2005–2006: Doctoral School of Material Science and Material Technologies,  
researcher  
2005–2006: Institute of Physics, University of Tartu, engineer  
2003–2005: Laser Diagnostic Instruments Ltd, researcher  
2002–2006: Institute of Physics, University of Tartu, Laboratory of Laser  
Techniques Ph.D. student

## **Scientific work**

Main field of research: Laser physics and laser-optical technologies  
Number of publications: 12

## **Awards**

2002 Estonian Academy of Sciences, student award  
2002 Estonian Education Ministry, student award  
2003 Estonian Physical Society, student award  
2003 Estonian Education and Research Ministry, student award

# CURRICULUM VITAE

## Sergei Štšemeljov

Sünniaeg ja koht: 14.12.1977, Narva, Eesti  
Kontakt aadress: Füüsika Instituut, Tartu Ülikool, Riia 142, 51014 Tartu, Eesti  
Telefon: +372 56675736  
E-mail: sergeys@ldi.ee

## Haridus

2000–2002: M.Sc. (optika ja spektroskoopia), Tartu Ülikool  
1996–2000: B.Sc. (eksperimentaalfüüsika ja infotehnoloogia), Tartu Ülikool  
1993–1996: Tartu Ülikooli Täppisteaduste kool  
1985–1996: Narva Kesklinna Gümnaasium

## Töökogemus

2006– Laser Diagnostic Instruments AS, teadur  
2005–2006: Tartu Ülikooli Materjaliteaduse ja Materjalide Tehnoloogia Doktorikool, erakorraline teadur  
2005–2006: Tartu Ülikooli Füüsika Instituut, insener  
2003–2005: Laser Diagnostic Instruments AS, teadur  
2002–2006: Tartu Ülikooli Füüsika Instituut, doktorant

## Teadustegevus

Peamine töösuund: Laserfüüsika ja laseroptilised tehnoloogiad  
Publikatsioone: 12

## Teaduspreemiad

2002 Eesti Teaduste Akadeemia, üliõpilaspreamia  
2002 Haridusministeerium, üliõpilaspreamia  
2003 Eesti Füüsika Selts, üliõpilaspreamia  
2003 Haridus- ja Teadusministeerium, üliõpilaspreamia